ASTRONOMY AND ASTROPHYSICS

Interstellar dust models for extinction and emission

F.-X. Désert[1,3], F. Boulanger[2,4], and J.L. Puget[2]

[1] Laboratory Astrophysics, Huygens Laboratorium, N. Bohrweg 2, Postbus 9504, NL-2300 RA Leiden, The Netherlands
[2] Groupe de Radioastronomie de l'E.N.S., 24 rue Lhomond, F-7-5231 Paris Cedex 5, France
[3] DEMIRM, Observatoire de Meudon, F-92195 Meudon, France
[4] IPAC, Caltech 100-22, Pasadena CA 91125, USA

Abstract. A large fraction of the power radiated by dust in the interstellar (IS) medium is observed in the near and mid infrared ($\lambda \lesssim 80 \mu m$). This emission is a strong evidence for very small grains in the interstellar medium from a few tenths to a few tens of nanometer radius. This interpretation implies a major revision of earlier dust models that were mainly based on the properties of the interstellar extinction curve. We propose a new coherent interpretation of both the interstellar extinction and the infrared emission, using an empirical dust model made of three components: big grains, very small grains (3-dimensional) and PAHs (2-dimensional). We argue that the big grain component is probably made of a size distribution of silicates with some dark refractory mantle and very small grains are probably carbon dominated. Allowing the dust abundances and sizes to be fixed by the average interstellar extinction curve and emission spectrum in the Solar neighbourhood, we investigate the variations of IR colours with the intensity of the incident radiation field in various astrophysical situations, in order to assess the validity of the model. We predict some correlations between anomalous extinction curves and anomalous infrared colours. Extensive tables and figures are given in order to facilitate comparison with observations.

1. Introduction

The wealth of infrared (IR) observations over the entire sky with a few arcminutes of resolution, provided for the first time by the *Infrared Astronomical Satellite* (IRAS), as well as near-infrared (NIR) ground-based and balloon-borne observations give a new powerful test of existing interstellar (IS) dust models (e.g. Mathis, Rumpl and Nordsieck 1977 (MRN), see also Draine and Lee 1984, Greenberg and Hong 1974, Hong and Greenberg 1980, and Rowan-Robinson 1986). In particular, there is strong evidence for very small grains and Polycyclic Aromatic Hydrocarbon molecules (PAHs) in the IS diffuse medium (Sellgren 1981, 1984,

Léger and Puget 1984). The fraction of the energy absorbed and reemitted by particles small enough to have temperature fluctuations is up to 40 percent of the total IR emission (Ryter, Puget and Perault 1987, hereafter RPP). The IS extinction curve has also been recently reanalysed (Greenberg and Chlewicki 1983, Fitzpatrick and Massa 1986, 1988) using multicomponent models (at least three). It is therefore important to investigate whether it is possible to put these new pieces of information together and if we can build a consistent picture of the interstellar dust. We try to satisfy the constraints given by both the extinction curve and the IR emission spectrum observed in the local IS medium. For example, using a modified MRN model, Draine and Anderson (1985) were short of explaining the $12 \mu m$ IRAS observations by at least a factor of five and produced an extinction curve with too large a bump (see also Weiland et al. 1986). Our approach is *not* to find the exact nature of IS grains although we suggest some possibilities, but to find: 1) the minimum number of different dust components; 2) the approximate parameters of the simplified grains optical properties that are needed to explain *simultaneously* the extinction and emission observations of the diffuse IS medium; and 3) to emphasise the consequences of the model when it is applied to various astrophysical environments.

After having reviewed the present status of the observations of the extinction curve and the IR emission, we deduce their basic implications for a simple dust model (Section 2). Then we try to quantitatively construct a "minimal" model using constraints coming from laboratory data and adjustments to the astronomical situation (Section 3). Applications of the model to different astrophysical environments are then considered (Section 4) and summarised (Section 5).

2. Observational constraints on interstellar dust models

2.1. The extinction curve

2.1.1. Observations

The extinction curve of the diffuse IS medium has been known for a few decades. It can be expressed in terms of a cross-section σ_H normalised to the number of hydrogen atoms (free or molecular). As a function of frequency, it rises from the IR to and through the visible, has a so-called bump at a constant wavelength of about 218 nm and rises again in the far ultraviolet

Send offprint requests to: F.-X. Désert[3]

(FUV). Recently, however, accurate determinations (with the *International Ultraviolet Explorer* (IUE) satellite) of the UV extinction curve towards a variety of stars (Seab, Snow and Joseph 1981, Greenberg and Chlewicki 1983, Fitzpatrick and Massa 1986, 1988) have revealed that three separate components were needed to explain the variability, from star to star, of the extinction curve : 1) a linear rise in the UV (linear in the wavenumber variable $x = 1/\lambda (\mu m^{-1})$; 2) the bump curve well approximated by a Drude profile (Fitzpatrick and Massa 1988); and 3) a non-linear rise in the FUV ($x \geq 5.9 \mu m^{-1}$). On the other hand, the linear rise in the UV has been shown to correlate very well with the near-infrared and visible rises of the extinction curve (Cardelli, Clayton and Mathis 1988, 1989). In particular the strength of this linear rise correlates with the parameter $R_V^{-1} = E_{B-V}/A_V$ measuring the slope of the visible rise.

2.1.2. Interpretation

a). Big grains of various compositions have been used to explain the NIR and visible rise of the extinction curve. Models where a size distribution is allowed (like the MRN model) are favored by the new observation that the UV linear rise correlates with the visible extinction. Grains invoked to explain the visible extinction (of size $a \sim 0.1 \mu m$) cannot provide the UV linear rise. Smaller grains ($\sim 0.01 \mu m$) are needed for that purpose and the concept of continuous size distribution seems unavoidable. A change in the size distribution $dN/da \propto a^{-\alpha}$ explains naturally the variation of R_V in different IS media as in the new composite model of Mathis and Whiffen (1989). The nature of these big grains is not completely known. Nevertheless, one can say that some silicates should be present in order to explain the absorption features observed in the IR extinction curve at 9.7 and 18 μm (e.g. Savage and Mathis 1979). Silicate optical properties have been computed by Draine and Lee (1984) using laboratory data and astronomical constraints. These authors show that bare silicate grains cannot provide the whole extinction in the visible because of their large albedo. This is the main reason why *big* graphite grains were suggested as the main absorbing particles in the visible (MRN). However the need for two types of particles to explain the visible extinction curve can easily be circumvented if we realise that "astronomical" silicate may not be bare but coated or mixed with a blacker material (probably carbon-dominated) as Chlewicki and Greenberg (1989) suggested (see also Mathis and Whiffen 1989, Duley, Jones and Williams 1989). We also notice that the width of the NIR absorption (9.7 and 18 μm) by astronomical silicates is larger than the width that can be obtained in laboratory experiments indicating the presence of abundant "impurities" in the astronomical silicates (Draine and Lee 1984). A further advantage of the existence of coated silicates is that it provides a natural explanation of the absorption feature observed towards the Galactic Centre at 3.4 μm (e.g. Savage and Mathis 1979, Butchart et al. 1986) by the C–H bonds in the silicates coatings (or "cement"). The general trend of the increase of R_V with the decrease of all three components of the UV extinction curve implies that the relative abundance of the UV producing grains is related to the grain size distribution (Cardelli, Clayton and Mathis 1989).

b). The bump carriers are still an object of controversy. They were originally thought to be small graphite particles ($a \leq 0.02 \mu m$, Stecher 1969, Gilra 1971) and included in the MRN model. However the latter model cannot explain the absence of variability of the peak wavelength of the bump in the astronomical extinction curve while its width varies (Greenberg and Chlewicki 1983, Fitzpatrick and Massa 1986). Draine (1988) has shown that small ($a < 20 nm$) oblate or prolate graphite grains can circumvent these difficulties. In another approach, from the conclusions of Fitzpatrick and Massa (1986), Hecht (1986) suggested that very small dehydrogenated carbon grains ($a \leq 5 nm$) should lead to a purely absorbing bump whose peak wavelength should be invariant as observed. In another development of the question, Sakata et al. (1983), Bussoletti, Collangeli and Orofino (1987), and De Groot et al. (1988) presented laboratory evidence that various forms of amorphous carbon dominated grains of very small size could indeed produce a bump at the observed wavelength, though with too broad a width. Although the precise identification remains uncertain, we will retain for our model that the bump carriers are very small and carbonaceous.

c). The FUV non-linear (hereafter FUVnl) rise has so far a very uncertain origin (e.g. Fitzpatrick and Massa 1988). It is known to have a constant curvature (Greenberg and Chlewicki 1983, Fitzpatrick and Massa 1988) and could be the foot of a second bump absorption around 70 nm that grain candidates usually show (Fitzpatrick and Massa 1988). We anticipate our discussion on IR emission (§2.2) and follow the idea (Léger et al. 1989c) that PAHs are possible candidates for this component of the extinction curve. It has been advocated that PAHs cannot produce a large portion of the extinction curve because the spectra of known PAH molecules show prominent sharp features at various visible and UV wavelengths (e.g. Hecht 1986, Salisbury et al. 1987). However a collection of PAH molecules has been shown to possess a rather smooth absorption curve (Donn and Krishna Swamy 1969, Léger et al. 1989c) because the individual features add up to a continuum if a sufficient number of PAH species coexist.

2.2. *The dust infrared emission*

2.2.1. Observations

In various interstellar environments, the infrared spectrum of extended regions is dominated by a broad far-infrared (FIR) component having a peak wavelength $\lambda \geq 100 \mu m$ in the local Solar neighbourhood IS radiation field (LISRF) moving to shorter wavelengths in the regions closer to heating stellar sources. This component is relatively well explained by the emission of grains at their equilibrium temperature ($T_e \leq 20 K$). However, in the last decade, there has been converging evidence that another component of the IS infrared emission coexists at shorter wavelengths ($\lambda \leq 80 \mu m$). First noticed by Andriesse (1978) in M 17, this short wavelength emission, that cannot be explained by grains at their equilibrium temperature, has been observed in a wide variety of regions including HII regions, planetary nebulae, reflection nebulae and galaxies as a whole (see e.g. Aitken 1981, Price 1981, Pajot et al. 1986b). Sellgren (1984) showed that the hypothesis of very small grains, which have a fluctuating temperature under the absorption of individual photons, could satisfactorily explain this IR component. Furthermore, the emission by reflection nebulae and HII regions between 3 and 13 μm is characterised by strong emission features at 3.3, 6.2, 7.7, 8.6 and 11.3 μm, the so-called unidentified IR (UIR) features.

The presence of short wavelength emission has received wide confirmations from IRAS observations of diffuse regions (see e.g. Beichman 1987, Puget and Léger 1989). The study of Boulanger and Pérault (1988) of high galactic latitude infrared emission (the so-called "cirrus" clouds) is used in the following because

Table 1. Cosecant law local IR emission

λ (μm)	Δλ (μm)	I_p/N_H (W/H)	Reference
3.3	0.05	2.5 ± 1.30 × 10^{-31}	1
12	5.7	1.1 ± 0.30 × 10^{-31}	2
25	9.8	0.7 ± 0.20 × 10^{-31}	2
60	31	1.1 ± 0.06 × 10^{-31}	2
100	35.6	3.2 ± 0.12 × 10^{-31}	2
102	30.6	2.5 ± 0.50 × 10^{-31}	3
137	48	3.9 ± 0.80 × 10^{-31}	3
262	94	7.2 ± 3.60 × 10^{-32}	3
325	250	7.1 ± 2.10 × 10^{-32}	4
870	296	6.5 × 2±1 × 10^{-34}	5

Notes to Table 1: λ is the central wavelength, Δλ is the filter full width at half maximum, and I_p is the in band power at the galactic poles deduce from cosecant law fitting. References are: (1) Giard et al. 1988: the feature is assumed to have a 0.05 μm FWHM and I_p/N_H is computed from the 12 μm IRAS band with the 3.3 to 12 μm scaling factor of the galactic plane (probably a lower limit); (2) Boulanger and Pérault 1988, (3) Lange et al. 1989, (4) Fabbri et al. 1986, (5) Pajot et al. 1986.

it represents the average dust IR emission in the diffuse HI gas of the Solar neighbourhood (see Table 1). The emission feature at 3.3 μm has recently been observed in the diffuse medium from balloon-borne instrument (Giard et al. 1988, 1989) confirming the widespread existence of the carriers of the family of features seen in reflection nebulae (Sellgren 1984).

These observations are supplemented in the submillimetre part with observations of the sky brightness at high latitudes by Fabbri et al. (1986) and by Lange et al. (1989) (see Matsumoto et al. 1988). We have also adapted the observations at 870 μm by Pajot et al. (1986a) of the inner Galaxy to an estimated column density of 1.25×10^{23} cm^{-2} (assuming a total $A_V = 50$) to get an estimate of IR dust emission at 1 mm (temperature effects should not be important at these wavelengths, hence the uncertainty estimated to be a factor 2) (Table 1).

2.2.2. Interpretation of the diffuse IR emission below ~ 15 μm

The PAH molecules have been identified as the likely carriers of the UIR features (Léger and Puget 1984, Puget, Léger and Boulanger 1985 (hereafter PLB), Allamandola, Tielens and Barker 1985). Additional evidence have then been accumulated (Léger and d'Hendecourt 1987) with the predictions and observations of weaker features at 3.4 μm (de Muizon et al. 1986), 5.2 μm (Allamandola et al. 1989), and near 12 μm (Cohen, Tielens and Allamandola 1985, de Muizon, d'Hendecourt, and Geballe 1989). Alternative explanations for the UIR features have been proposed by Sakata et al. (1984) who suggested that quenched carbonaceous composites (QCC) could be the carriers. The model we develop in the next Section (which assumes PAHs as the UIR feature carriers) is not very dependent on the exact nature of the carriers *as long as they are very small grains that fluctuate in temperature.* The model by Duley and Williams (1988), in which amorphous carbon clusters are loosely bound to big grains, is incompatible with our assumptions and difficult to reconcile with the infrared data. Their model does not explain why the carbonaceous material seen in absorption at 3.4 μm is not seen in emission in the diffuse IS medium and the yield for near-infrared

2.2.3. Interpretation of the diffuse IR emission between ~ 15 and ~ 60 μm

Giard et al. (1988) have suggested that, in the diffuse IS medium, PAHs probably contribute to the 12 μm band of IRAS because there is a strong correlation between the intensity of the 3.3 μm feature and the 12 μm emission. However, the origin of the IR emission at longer wavelengths (25 and even 60 μm) has been less investigated, probably because of problems with the Zodiacal light subtraction and inaccessibility from ground-based observations. That this emission arises from very small grains (VSGs) has been clearly shown, for example, by Castelaz, Sellgren and Werner (1987) in the Pleiades. The IR colour between 12 and 25 μm does *not* change as the nebula is sampled toward larger distances from the illuminating star. Like the 12 μm emission, the 25 μm emission that is widely distributed in the diffuse medium has only increased to 0.26 compared with the ratio of 0.21 in high galactic latitudes (typical of the diffuse medium in the Solar neighbourhood) (Boulanger and Pérault 1988), cannot be explained by standard dust grains emitting at their equilibrium temperature (see e.g. Draine and Anderson 1985). There are some indications that, even in the 60 μm IRAS band, out-of-equilibrium processes can make a significant contribution. Analysing cirrus clouds at 5 kpc from the Galactic Centre, Pérault et al. (1989) conclude that the 60 to 100 μm flux ratio does not decrease as fast as predicted by standard dust models. Walterbos and Schwering (1987) reach the same conclusions for the dust in the nearby Andromeda galaxy, where the 60/100 μm flux ratio has a remarkably constant value of about 0.20 in a large fraction of the galaxy. In order to emit beyond ~ 25 μm, the PAH molecules (*i.e.* 2-dimensional grains) would have to be uncomfortably big (a number of carbon atoms larger that ~ 1000). This is the reason why we suggest that 3-dimensional VSGs are reasonable candidates for the 25 and part of the 60 μm emission. We cannot exclude very small silicates as the emitters at these wavelengths (as was done at 12 μm by Désert et al. 1986) because spectroscopic observations of the diffuse medium do not exist at the moment (a good test of their presence would be the observations of the 18 μm silicate feature in *emission* in the diffuse medium). Similarly VSGs with other chemical composition (metallic or metallic oxide) cannot be ruled out as suggested by Chlewicki and Laureijs (1988), although the latter authors assume a thermal emission from very small iron grains without temperature fluctuations. However, we suggest in Sect. 3 that carbon-dominated VSGs meet in a better way the energetical constraints between the extinction curve and the IR emission spectrum of the IS diffuse medium and are likely to be the dominant VSGs in our local IS medium.

2.2.4. Interpretation of the diffuse far IR emission

As for wavelengths longward of 100 μm the data are so scarce that we still do not know exactly: 1) what the emissivities are (see e.g. Hildebrand 1983, Pajot et al. 1986a), though a steep emissivity law ($Q_a \propto \lambda^{-1.5,-2}$) is favored in the following; and

emission to total emission, measured or predicted on the basis of presently measured conductivities is weak.

2) whether one or two dust components coexist as the main emitters at long wavelengths, as in the MRN model (see Draine and Anderson 1985).

3. An "astronomical" dust model

3.1. Gathering the pieces

From the last section, the analysis of the extinction curve has yielded the clue that at least 3 components of dust exist in the IS medium: "FUV" particles, "bump" particles and "big" grains. Another clue is given by the interpretation of the IR emission spectrum: 2 dust components have to be small enough ($a \leq 10$ nm) in order to emit at short wavelengths ($\lambda \leq 80 \mu m$) by the temperature fluctuation mechanism (the near IR (NIR) and mid IR (MIR) components, see Sect. 2.2.2 and 2.2.3) and another more traditional component provides the maximum emission in far IR wavelengths. Before modeling the optical properties of each component, we must attribute to each component in the extinction curve, a component in the IR emission. For that purpose, we will rely on additional observations and laboratory measurements that partly elucidate the question.

The FUV component is likely to be associated with the NIR component i.e. PAHs because: 1) the Red Rectangle nebula, where the UIR features are detected (Cohen et al. 1975) shows a very weak bump in the extinction curve (Sitko, Savage and Meade 1981) but has a large non-linear UV rise (other examples include NGC 7023 and the Pleiades : Cox and Leene 1987 (and references therein); 2) the nebula around σ Sco shows a lack of NIR emission (as measured by its IRAS 12 μm flux) at the nearest locations to the star (RPP), and this lack is associated with the absence of FUV rise of the extinction curve toward σ Sco (Bless and Savage 1972); 3) there is no correlation between the bump parameters and the 12 μm emission relative to the FIR emission in a sample of stars studied by Cox and Leene (1987) and Leene and Cox (1987); and 4) laboratory measurements (Léger et al. 1989c) of the extinction curve due to a mixture of PAHs (coal tar) have revealed a large non-linear rise in the FUV (although it also shows an additional broad weak bump around 220 nm).

The bump particles are therefore likely a contrario to be those which produce the MIR emission which implies that the particle size is of the order of several nanometers. We call these bump particles VSGs and we know that they are probably carbon-dominated (Sect. 2.1.2b).

As there is no observational evidence that two distinct components of big grains (BGs) are needed to explain the IR and visible extinction curve (in the diffuse medium at least), as was assumed by MRN, we will attempt to build a dust model with only one type of big grains (BGs) that produce the extinction curve in the NIR, visible (and the additional linear UV rise, see Sect. 2.1.2a) and the FIR emission. These big grains are dominated in mass by the silicates with an additional coating (Hong and Greenberg 1980) or cement (Mathis and Whiffen 1989) which is mainly made of carbon and is responsible for the observed 3.4 μm absorption feature (seen e.g. towards the Galactic Centre).

In Sect. 3.2, we investigate the likely optical properties of the three dust components we have suggested. We deduce the abundance in mass of each component Y_{PAH}, Y_{VSG} and Y_{BG} relative to hydrogen, by using the balance between the energy absorbed by the grains embedded in the LISRF as modeled by

Pérault et al. (1989) and their IR emission as summarised in Table 1. The IR emission of each type and size of grains has been calculated by taking into account the grain temperature fluctuations using the formalism developed by Désert, Boulanger and Shore (1986), the heat capacity being given in the following. The energy step in the discretisation of the internal energy distribution of each grain has been taken as 0.15 eV, small enough to take into account the temperature fluctuations induced by NIR photons on the small grains.

3.2. "Astronomical" grain properties

3.2.1. The PAHs

As observed in the laboratory (Léger et al. 1989c), the PAH molecules can produce the FUVnl part of the extinction curve and some continuous extinction in the visible. The following argument shows that these two extinction components are both needed in order to account for the PAHs NIR emission in cirrus clouds. First, we convert the extinction function obtained by Fitzpatrick and Massa (1988) to a dust cross-section per H atom, using $R = 3.1$ and $A_V/N_H = 5.3 \times 10^{-22}$ cm² (Bohlin, Savage and Drake 1978). For the FUVnl component, we get:

$$\sigma_H(FUV nl) = 2.3 \times 10^{-23} f_u(x) \, \text{cm}^2/\text{H},$$ (3.2.1)

with

$$f_u(x) = (x - 5.9)^2 (0.1x + 0.41) \quad \text{for} \quad x \geq 5.9 \, \mu m^{-1}$$
$$= 0 \quad \text{otherwise,}$$ (3.2.2)

where $x = 1/\lambda \, (\mu m^{-1})$ (all the numbers in parenthesis are in μm^{-1}). When integrated over x, the product of the cross-section times the LISRF gives the specific power absorbed by the PAHs: $P_H(FUV nl) \simeq 0.40 \times 10^{-31}$ W/H. Hence, the FUVnl part of the extinction curve is not large enough to explain the emission in the NIR by PAHs, where at least a specific power 1.0×10^{-31} W/H is emitted (Table 1). A visible-UV continuum has to be part of PAH absorption cross-section as well as the FUVnl component (e.g. the coronene has a broad feature at 300 nm). This cross-section is cut off at a frequency depending on the size of the molecule $x < x_c = 1.25 (a/1 \, \text{nm})^{-1}$ (Platt 1956, PLB) because of the quantization of electronic levels of neutral PAHs. An analytical representation of the PAH cross-section is given in Appendix A. The mass abundance of PAHs Y_{PAH} has been calculated in order to explain eq. (3.2.1) (actually BGs produce a negative non-linear UV rise which is taken into account too, see Fig. 2) and to be consistent with the typical values of PAH absorption cross-sections obtained in laboratory by Léger et al. (1989c) (although measured PAHs have a radius of at most 0.4 nm).

The IR properties of PAHs are adapted from PLB and Léger and d'Hendecourt (1987). The cross-section of PAHs results from the contribution of three terms (see Appendix A) : 1) the electronic continuum which is, for big molecules, an infrared extension of the visible and UV cross-section, 2) the main features at 3.3, 6.2, 7.7, 8.6, and 11.3 μm for which the integrated cross-sections are given by Léger, d'Hendecourt and Défourneau (1989b hereafter LHD) (throughout this paper, we assume a dehydrogenation of 40%) and the number of carbon atoms and hydrogen sites are given respectively by $N_C = 120 (a/1 \, \text{nm})^2$ and $N_H = \sqrt{6} N_C$, and 3) a pseudo-continuum below these features at wavelengths larger than about 10 μm that is due to numerous weak features

(LHD) the wavelength of which depends on the particular PAH molecule. Some parameters in the analytical representation of PAHs, because it is thought to represent less than about 20% of the total IR emission of PAHs (Ryter and d'Hendecourt 1989, Guhathakurta and Tyson 1989); the ionization energy is assumed to stay in PAHs (although some fraction goes with the photoelectron to heat up the gas, d'Hendecourt and Léger 1986). Finally, the heat capacity of PAHs is derived from Léger and d'Hendecourt (1987); it is close to that of graphite. Greenberg and Chlewicki (1983, see their Appendix) have shown that the FUV rise must be independent on the size of the grains (here the PAHs). It is not yet known whether the resonance in the UV at around 70 nm (also seen in graphite) which probably explains the FUVnl rise (for $x \geq 6\,\mu m^{-1}$ depends on the size of PAHs. This resonance is interpreted as an ionisation curve in the PAH hypothesis.

3.2.2. The very small grains

As deduced in Sect. 3.2, the VSGs are here assumed to produce the absorption bump at 220 nm and the mid-infrared emission. Following Fitzpatrick and Massa (1986), we model the bump with a Drude profile with a peak at $x_0 = 4.6\,\mu m^{-1}$ and a width of $\gamma = 1.0\,\mu m^{-1}$. All the possible candidates for the bump carriers (Bussoletti et al. 1987, Sakata et al. 1984, De Groot et al. 1988, Draine 1988) show the presence of an underlying continuum that we model as linear in $x = 1\,\mu m/\lambda$. We have thus adopted the following absorption efficiency:

$$\frac{Q}{a} = \left(6.6 \times 10^4 x + \frac{1.92 \times 10^6 x^2}{[(x^2 - x_0^2)^2 + \gamma^2 x^2]}\right)\,cm^{-1}, \quad (3.2.3)$$

where the strength of the Drude profile has been scaled to match that of small graphite grains (Draine and Lee 1984). As in Sect. 3.2.1, we can calculate the power absorbed in the bump only (i.e. without any continuum): $P_H(\text{Bump}) \simeq 0.43 \times 10^{-31}$ W/H. However the power emitted by dust in the wavelength range of 20 to 70 μm is estimated to be $\simeq 0.9 \times 10^{-31}$ W/H from Table 1. This allowed us to set roughly the strength of the continuous component behind the Drude profile in formula (3.2.3). An abundance of $Y_{VSG} = 4.7 \times 10^{-4}$ is needed to account for the average bump in the IS medium. The bump-to-continuum ratio is comparable to the graphite one and relatively large when compared with that of very small amorphous carbon grains suggested by Bussoletti, Colangelli and Orofino (1987) or Sakata et al. (1984). The formula (3.2.3) is taken as representative of VSGs even down to infrared wavelengths because it is consistent with amorphous carbon grain absorption efficiencies (e.g. Borghesi, Bussoletti and Colangelli 1985) and theoretical expectations for VSGs (i.e. of radius less than 10nm: Seki and Yamamoto 1980). We have assumed that the heat capacity is approximated by a Debye model with $T_D = 2200$ K.

3.2.3. Big Grains

If silicates have a coating of mainly carbon material or are mixed with it, one can expect that their absorption efficiency will be increased relative to the bare silicate ones. This modification of the silicate efficiencies is required on energetical grounds. In order to keep the model as simple as possible we adopt the following absorption and scattering efficiencies (ratios of cross-section to geometric area) which reproduce typical efficiencies of grains when wavelengths are comparable to the grain radius (van de Hulst 1957), although we neglect some oscillating behaviour which are radius dependent:

$$Q_a = Q_{am} u \quad \text{for} \quad u \leq 1$$
$$= Q_{am} \quad \text{for} \quad u > 1, \quad (3.2.4)$$

with
$$u = \frac{2\pi a}{\lambda}$$

and
$$Q_s = Q_{sm} u^4 \quad \text{for} \quad u \leq 1$$
$$= Q_{sm} \quad \text{for} \quad u > 1. \quad (3.2.5)$$

Imposing that $Q_{am} + Q_s = 2$ and for the size distribution described in Sect. 3.3, we need a maximum albedo $\beta_m = Q_{sm}/(Q_{sm} + Q_{am})$ of about 0.6 for the big grains to emit the power observed in the FIR region (Table 1). The absorption efficiency in (3.2.4) is then smoothly joined (at around 8 μm) to the typical values of 0.9 for bare silicates. The IR efficiencies of silicates deduced by Draine and Lee (1984) who assumed a steep emissivity ($Q_a \propto \lambda^{-2}$) in the FIR region (Andriesse 1974) (see however next Section). The heat capacity has been assumed to follow the relation for silicates given by Léger, Jura and Omont (1986). This parameter is not critical because the temperature of BGs does not fluctuate by more than 1 K when $a \geq 25$ nm in the LISRF, and therefore BGs can be considered to emit at their equilibrium temperature.

3.3. The grain size distributions

For each dust components the grain size distribution is modelled as a power law where the number density of grains of radius between a and $a + da$ is:

$$n(a) \propto a^{-\alpha} \quad \text{between} \quad a_{min} \text{ and } a_{max}. \quad (3.3.1)$$

We have explored various possibilities for the mass abundance Y and the distribution parameters (α, a_{min} and a_{max}) for each dust component in order to find a good simultaneous match of the extinction curve and the IR spectrum of the local IS medium. In the following, we discuss these constraints for each component before giving the global features of the dust model we have derived. The power-law distribution has been chosen for its convenience in parametrisation.

3.3.1. PAHs size distribution

The IR emission has been computed for dust embedded in the local ISRF (LISRF) as given by Perault et al. (1989), which is similar to the one by Mathis, Mezger and Panagia (1983). We have first dealt with the case of a small optical thickness ($\tau \ll 1$) at all wavelengths. The more complicated cases, which occur near a cloud for example, will be studied in a subsequent paper (Bernard et al. 1990).

The PAHs size distribution is mainly constrained by the different near-infrared properties of PAH molecules of different sizes. The minimum size is taken as the size a PAH must have to survive
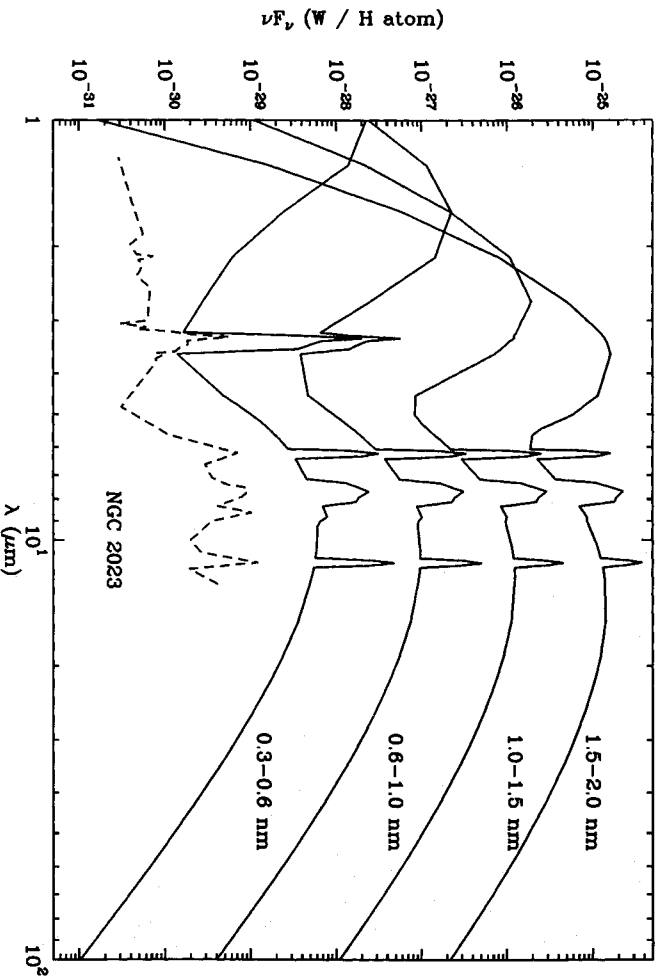
220

Fig. 1. IR spectra of different size distributions when exposed to the radiation field of a B3 star at 0.15 pc, the distance at which the spectrum of the reflection nebula NGC 2023 has been measured by Sellgren et al. (1985) (dashed curve, arbitrary scale). Each curve is log-shifted from the previous one by a factor 10. The lower curve corresponds to the PAH abundance and size distribution of Table 2. PAHs are assumed to be fully ionised in reflection nebulae (d'Hendecourt and Léger 1987). Note the variations of the feature-to-continuum ratio at 3.3 μm (see text).

photo-thermo-dissociation (Léger et al. 1989a, Omont 1986): around 0.4 nm in the local neighbourhood. The maximum size is less constrained. However, as the radius becomes larger than about 1.1 nm the ratio of emissions at 25 μm to 12 μm becomes larger than observed in the LISRF. We can therefore set an upper limit at around 1.2 nm.

The size distribution can also be constrained by the analysis of the well-studied case of the reflection nebula NGC 2023 (Sellgren et al. 1983, 1985). Although the PAHs in the nebular cloud have been processed by the strong stellar radiation field, we think that at least the largest PAHs should have survived the strong radiation field. Indeed, we have computed the emission of PAHs of different sizes when embedded in a B3 stellar radiation field ($L = 8 \times 10^3 L_\odot$, $T_{eff} = 2 \times 10^4$ K at a distance of 0.15 pc, in the HI medium, see Sellgren et al. 1983). Figure 1 shows the PAH emission in the NIR, when a_{min} and a_{max} are chosen respectively as (0.3, 0.6 nm), (0.6, 1.0 nm), (1.0, 1.5 nm) and (1.5, 2 nm) with the exponent $\alpha = 2$. We see that as the mean size of PAHs increases, the 3.3 μm feature intensity decreases relative to the underlying continuum. From the comparison with the observed nebular spectrum we deduce: 1) that the largest size of the PAHs is of the order of 1.5 nm; and 2) that the 3.3 μm feature-to-continuum ratio depends on the size distribution of PAHs. Sellgren et al. (1983) and Gatley et al. (1987) have indeed noticed some variations of the feature-to-continuum ratio across the nebula (by a factor of 2). The ratio drops near the ionizing star. We interpret these observations as indicating a spatially varying mean size of PAHs, the largest being the more resistant to the radiation field. The same effect is observed in the Orion Nebula (Sellgren 1981).

3.3.2. VSG size distribution

The 25 to 60 μm flux ratio of VSGs can be deduced by assuming that about half the observed fluxes at both 25 and 60 μm are due to VSGs while the other half is due to PAH emission at 25 μm (this assumption will be discussed in Section 4.3) and big grains

at 60 μm (see §2.3). We obtain that VSGs must approximately satisfy $R_{23} = I_\nu(25 \mu m)/I_\nu(60 \mu m) = 0.26$. This ratio is very dependent on the size of the VSGs: 0.77, 0.54, 0.38, 0.25, 0.16, 0.099 for respectively $a = 4.4, 5.2, 6.1, 7.2, 8.5, 10$ nm. Therefore, the R_{23} ratio constrains the average size of VSGs to be about 7 nm.

Given the average size, the minimum and maximum sizes and the exponent of the size distribution are not very well constrained either by the extinction curve, because VSGs are optically thin at all wavelengths up to the UV, or by the IR data (negligible contribution to 12 and 100 μm). In order to have fewer free parameters to fix, we have therefore assumed that the whole grain size distribution is continuous from one grain component to the next. Hence we have imposed: $a_{min}(VSG) = a_{max}(PAHs)$ and $a_{max}(VSG) = a_{min}(BG)$. The exact contribution of the VSGs to the 60 μm IRAS band is crucial to our understanding of the FIR colour variations with different radiation field intensity as further discussed in Section 3.3.4.

3.3.3. BGs size distribution

Constraints on the size distribution of the big grains mainly come from the extinction curve. The minimum size is well determined by the FUV linear rise (see §2.1.2): $a_{min} \simeq 10$ to 20 nm. On the other hand the maximum size should be at least about 100 nm and the exponent $\alpha \simeq 2.7 - 3.5$ in order to explain the NIR and visible extinction level and shape ($a_{max} \geq 0.55 \mu m/2\pi$). Polarization of light (although not explicitly included in this paper) requires grain sizes of around 0.1 μm too. The exponent α and the maximum size a_{max} are directly related to the selective extinction $R = A_V/E(B - V)$ (see similar conclusions by Mathis and Whiffen 1989). Typical BG maximum albedos β_m between 0.55 to 0.7 have been chosen to match the energy constraints principally given by the 100 μm emission. Chlewicki and Greenberg (1989) have shown that dielectric grains must not be pure scatterers in order to produce the polarization of light, in agreement with our relatively low albedo.

Table 2. Adopted model of interstellar dust

Component	$Y = m/m_H$	α	a_{min} nm	a_{max} nm	ρ	β_m
PAH	4.3×10^{-4}	3	0.4	1.2	2.4×10^{-7} g cm^{-2}	0
VSG	4.7×10^{-4}	2.6	1.2	15	2.3 g cm^{-3}	0
BG	6.4×10^{-3}	2.9	15	110	3.0 g cm^{-3}	0.61

Notes to Table 2: Y is the mass abundance relative to hydrogen (Helium is not included); α is the exponent of the power-law size distribution between a_{min} and a_{max} (see formula 3.3.1); β_m is the maximum albedo (formula 3.2.6) and ρ is the mass density of the material (PAHs are 2-dimensional).

3.4. The choice among possible dust models

The various constraints imposed by astronomical observations, laboratory data and physical consistency are *not* sufficient, in their present state, to lead to a unique model for the diffuse IS dust. In particular, *IRAS* observations, although sensitive, were made with only four distinct broad bands, and the submillimetre data for the diffuse medium are very scarce. Nethervless, no previous dust model has satisfied the constraints enumerated above, hence we need *at least one* model that could be used for comparison with observations. The method we used to derive a consistent dust model is: 1) to adopt a set of parameters (abundance and size distribution, albedo β_m of big grains) in order to fit the extinction curve; 2) to compute the energy degradation from the visible and UV to the IR by the grains, when they are embedded in the LISRF; 3) to compare the obtained IR spectrum with the values given in Table 1; and last 4) to optimise the parameters and start 1) again in order to obtain a satisfying agreement with the data. Some of the conclusions in §3.3 were reached that way. It appears also that a whole class of "solutions" is obtained, which cannot be separated directly by this method. The main reason lies in the insufficient observations at the wavelength of the peak of the IR spectrum ($100 \leq \lambda \leq 200\,\mu m$) which is outside the *IRAS* bands. Therefore, we have used the additional constraints provided by *IRAS* observations of cirrus clouds at 5 kpc from the Galactic Centre which are heated by stars in the molecular ring (Pérault et al. 1989). As discussed in §3.1, the 60/100 μm intensity ratio has risen from 0.21 in the Solar Neighbourhood to only 0.27 for the 5 kpc-cirrus whereas the power emitted at 100 μm has risen by a factor of 7. One model is now presented which satisfies this additional constraint. For that purpose, the BGs emissivity in the far IR has been slightly modified such that it is proportional to $\lambda^{-1.5}$ from the silicate band at 20 μm up to 100 μm then proportional to λ^{-2} in the submillimetre wavelengths. The normalisation is $Q/a = 246$ cm^{-1} at $\lambda = 100\,\mu m$. Such a modification is minor compared with the variability of the emissivity of different samples of silicate grains (see, for example, Hasegawa and Koike 1984) and it is consistent with layer-lattice silicates (Tielens and Allamandola 1987).

3.5. The resulting extinction and IR emission

Figure 2 shows the extinction curve obtained by the optimised grain distribution of Table 2. The standard observed extinction curve, as given by Savage and Mathis (1979) in Figure 2 (crosses), is explained by the present dust model. Moreover, anomalous extinction curves can be naturally obtained by independently varying the size distribution and abundances of one or several dust components in the direction noticed by Fitzpatrick and Massa (1988) (see Section 4).

The extinction curve in the NIR is slightly different from the observations by Rieke and Lebofsky (1985) (Figure 3) probably because of our simplistic assumptions for BGs absorption behaviour with wavelengths (§ 3.2.3). We notice that the PAH molecules do not produce any noticeable absorption features in the NIR extinction curve (see LHD), although the near IR emission is dominated by them (see the discussion by Puget and Léger 1989). The theoretical behaviour of the emissivities in the submillimetre is satisfied: $\epsilon \propto \lambda^{-1}$ for small grains ($a \leq 10$ nm) and $\epsilon \propto \lambda^{-2}$ for big grains (Andriesse 1974, Seki and Yamamoto 1980).

Figure 4 and Tables 3 and 4 show the IR emission by each dust component and the total IR spectrum (continuous line). The salient features are that: 1) a broad plateau of emission spans the wavelengths from 2 to 60 μm; 2) the presence of PAHs is fundamental to explain a third of the total IR emission; 3) the BG component accounts for 90 percent of the total 100 μm *IRAS* emission and all the sub-millimetric measurements, hence sub-millimetric observations cannot be used to determine PAH and VSG masses (but these masses are only a small fraction of the total mass of solid particles: 13% in Table 2); 4) the peak infrared emission occurs at longer wavelengths ($\sim 140\,\mu m$) than could be observed by *IRAS*; rocket observations by Lange et al. 1989 indeed confirm this predicted IR peak of the IS dust emission; and 5) a third component (called VSGs) made of intermediate size particles is difficult to avoid in order to explain quantitatively the infrared spectrum between 20 and 80 μm as clearly observed by *IRAS* for the first time.

Figure 5 shows the mass spectrum of dust as a function of radius ($a\,dm/da \propto a^{q+1-\alpha}$ where $q = 2$ for PAHs and $q = 3$ for VSGs and BGs). The local minimum in the infrared spectrum at about 25 μm (Fig. 4) is reflected in Fig. 5 as a relative deficit of particles of sizes between 2 and 4 nm. One can notice the qualitative similarity between Figure 4 and 5.

The "drawback" of having simultaneously fit the extinction curve and the IR emission can be seen in Figure 6 where the effective albedo β of interstellar dust is plotted against the wavenumber x (continuous line). Although the shape of the curve is in agreement with the albedos measured by Lillie and Witt (1976: see in particular the minimum of the albedo at the wavenumber of the bump feature), the general level (about 0.4) that we predict is fifty percent lower. The agreement seems better with the observations by Laureijs, Mattila and Schnur (1987)
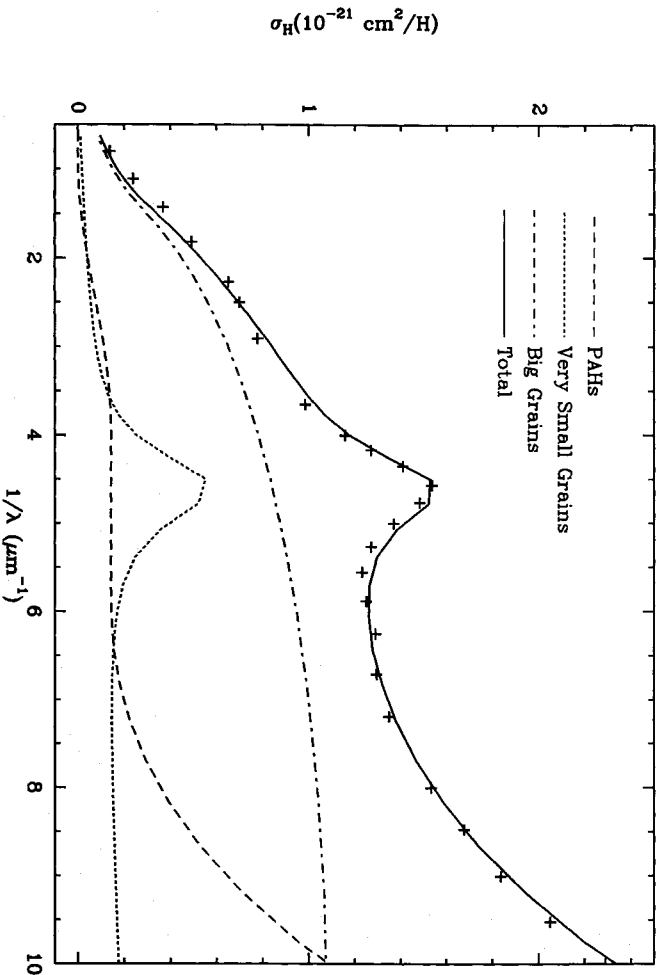
222

Fig. 2. Extinction curve of the diffuse medium in the visible and UV. The curves are drawn from the model described in Section 3. The crosses represent the observed average extinction curve from Savage and Mathis (1979) normalised to hydrogen atoms with $R = 3.1$ and $N_H/E(B-V) = 5.8 \times 10^{21}$ H/cm².
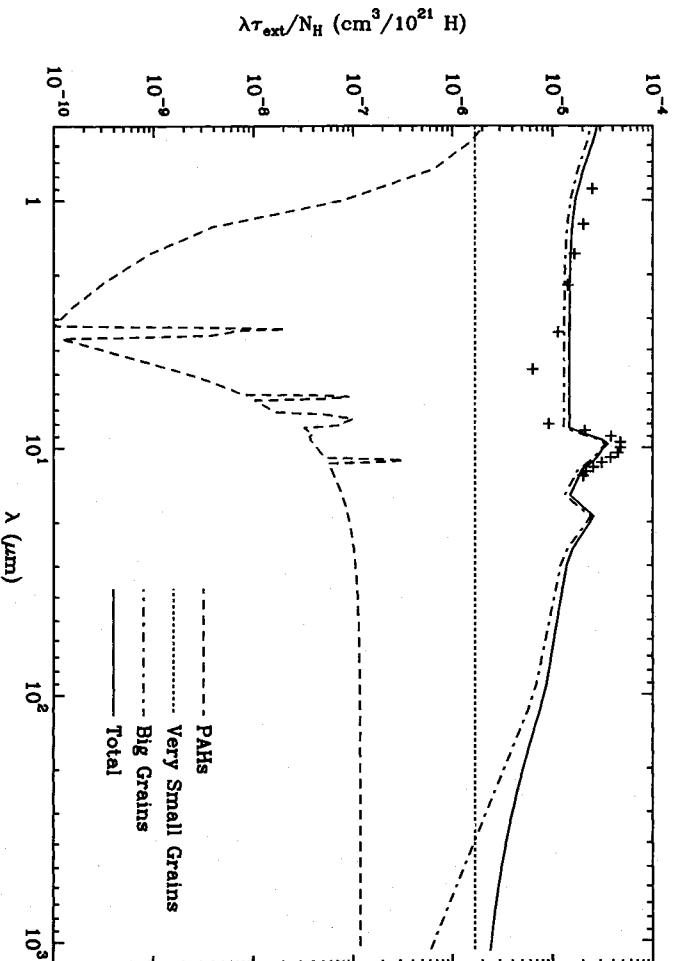

Fig. 3. Extinction curve of the diffuse medium in the infrared. Data (crosses) from Rieke and Lebofsky (1985) are normalised like in the previous figure, but the units are different. Note that PAHs do not contribute at all to the IR extinction curve. The 3.4 μm absorption band due to C-H stretching on big grain mantles is not shown here although it is part of the present dust model.

of an isolated cloud (Lynds 1642) – see also some observations by Morgan (1980). The energetical constraints prevent any dust model from explaining the whole IR spectrum if the effective albedo is above 0.5 (unless the LISRF is stronger than the one used here by a factor of at least 50%). Indeed, if albedos from Lillie and Witt (1976) are used in conjonction to the LISRF to compute the total power absorbed by dust, one gets less than about 4.5×10^{-31} W/H as compared with the value 6.9×10^{-31} from Table 4. That is the *basic reason* why previous dust models could not be simultaneously consistent with the existing IR data (e.g. Draine and Anderson 1985, Rowan-Robinson 1986) and the

extinction curve. As measurements of dust albedos are extremely difficult and geometry dependent (Savage and Mathis 1979, Chlewicki and Greenberg 1984), we think that the IR constraint is more important to satisfy than uncertain albedos. The conclusion that albedos must decrease in the far UV has been independently reached by LHD who also use PAHs for the FUV extinction rise.

The abundances of PAHs and VSGs (cf. Table 2) correspond each to about 8 percent of the cosmic abundance of carbon ($m_C/m_H = 5.8 \times 10^{-3}$, Meyer 1979). However, some carbon is locked up in BGs too (see Section 2.1.2). From the 3.4 μm
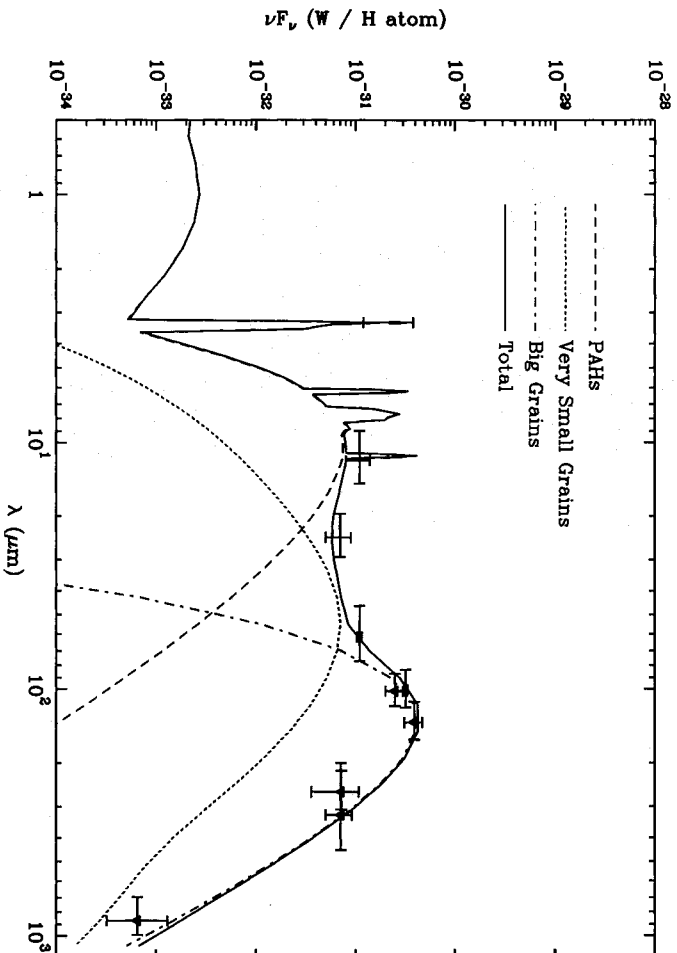
Fig. 4. Dust emission spectrum. Observations (crosses) pertain to the "cirrus" interstellar diffuse medium (see Table 1 and text). The horizontal bars represent the filter width used in the observations (given in Table 1). The model resulting spectrum (continuous line) is the sum of the three components that are PAHs, VSGs, and BGs.

Table 3. IR emission of dust in the solar neighbourhood

| λ µm | 12 | 25 | 60 | 100 | 200 | 400 | 800 | K(2.2) | L'(3.3) |
Band#	1	2	3	4	5	6			
PAH	3.12(-2)	1.90(-2)	4.23(-3)	1.11(-3)	1.49(-4)	1.43(-4)	3.06(-4)	1.22(-4)	1.82(-3)
VSG	1.77(-3)	2.06(-2)	1.06(-1)	1.22(-1)	5.88(-2)	1.61(-2)	7.19(-3)	9.23(-8)	3.02(-6)
BG	0.00(0)	2.11(-7)	6.62(-2)	7.45(-1)	1.48(0)	3.98(-1)	5.36(-2)	0.00(0)	0.00(0)
Total	3.30(-2)	3.96(-2)	1.76(-1)	8.68(-1)	1.54(0)	4.14(-1)	6.11(-2)	1.22(-4)	1.83(-3)

Colours	Γ_1	Γ_2	R_{54}	R_{64}	R_{14}	R_{24}	R_{34}
PAH	3.19(1)	9.33(0)	1.34(-1)	1.28(-1)	2.81(1)	1.71(1)	3.80(0)
VSG	4.94(-2)	2.76(-1)	4.81(-1)	1.31(-1)	1.45(-2)	1.69(-1)	8.65(-1)
BG	0.00(0)	9.86(-7)	1.99(0)	5.34(-1)	0.00(0)	2.83(-7)	8.90(-2)
Total	2.37(-1)	1.37(-1)	1.78(0)	4.77(-1)	3.80(-2)	4.57(-2)	2.03(-1)

Notes to Table 3: The IR L_ν/N_H specific emission is in MJy/sr/10^{20}Hcm^{-2} units and corresponds to an emission at the centre wavelength of an assumed constant νL_ν spectrum (see *IRAS Explanatory Supplement* 1985) for IRAS filters and Rayleigh-Jeans spectrum for K and L' filters. Zero width has been assumed for submillimetre wavelengths. $\Gamma_{1,2} = \nu L_\nu(12,25)/(\nu L_\nu(60) + \nu L_\nu(100))$ and $R_{ij} = L_\nu(\text{band}_i)/L_\nu(\text{band}_j)$.

properties of the "astronomical" grains directly correspond to uncertainties in the abundances. Tables 3 and 4 summarise the IR broad band specific fluxes and luminosities of each dust component as well as their sum. We see that *IRAS* bands encompass only 43 percent of the total luminosity of interstellar dust embedded in the LISRF (Pérault et al. 1989).

absorption feature measured towards the Galactic Centre, Tielens and Allamandola (1987) have estimated to 24 percent the carbon locked up on BGs. More than 70 percent of Si, Mg and Fe are needed to build up the BGs. Hence, the proposed model satisfies the cosmic abundance constraint, although we do not put too much emphasis on this result because uncertainties in the optical
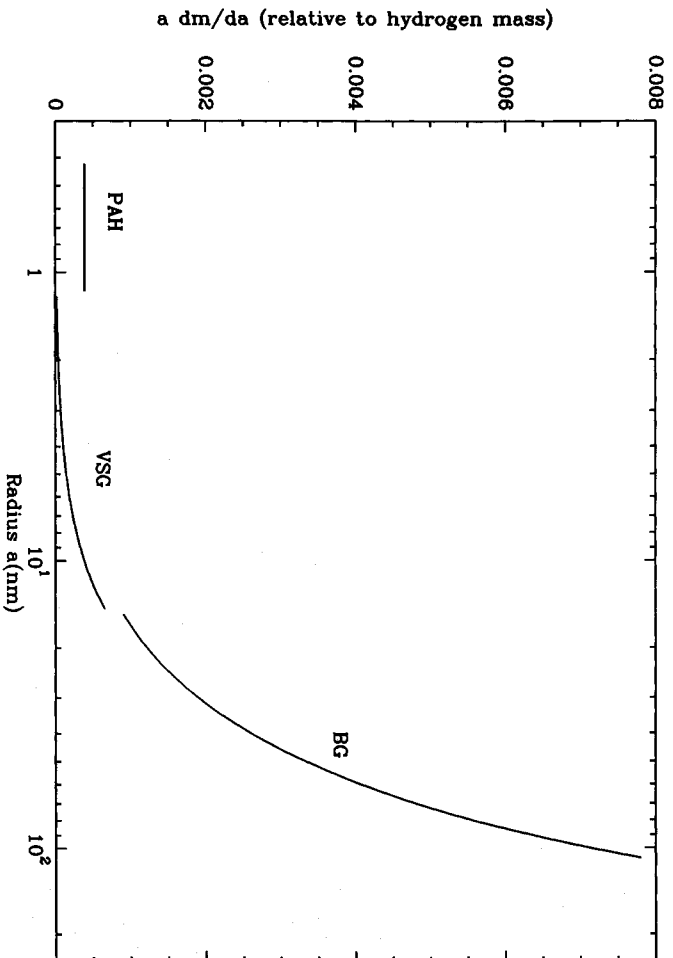
Fig. 5. Dust mass spectrum. The area under the curves represents the mass of dust for a unit hydrogen mass.
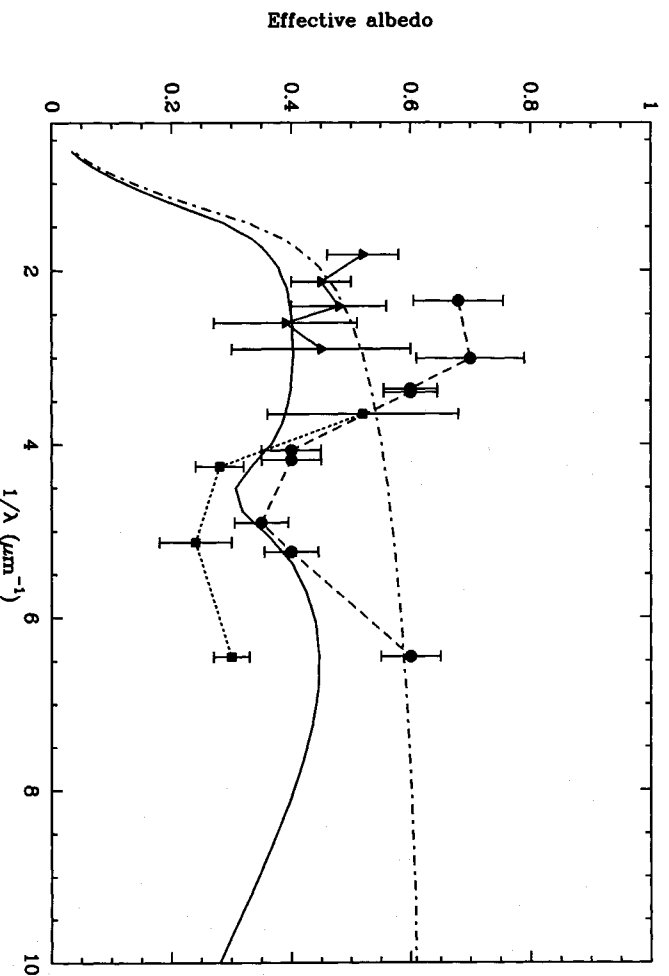
Fig. 6. Dust albedo in the visible and UV spectrum. The model (continuous curve) is compared to observations by Lillie and Witt (1976, circles), Chlewicki and Laureijs (1988, triangles), and Morgan (1980, squares). Big grains only (dot-dashed curve) have an albedo saturating at 0.61.

Table 4. IR luminosities of dust in the solar neighbourhood

	L_{tot}	L_{iras4}	$L_{3.3f}$	$L_{irastot}$	$L(5-1000)$	$L(10-120)$
PAH	1.37(-31)	4.19(-34)	5.80(-33)	1.30(-31)	1.28(-31)	6.58(-32)
VSG	1.20(-31)	4.61(-32)	0.00(0)	1.49(-31)	1.20(-31)	1.03(-31)
BG	4.34(-31)	2.81(-31)	0.00(0)	3.22(-31)	4.34(-31)	1.29(-31)
Total	6.92(-31)	3.27(-31)	5.80(-33)	6.01(-31)	6.82(-31)	2.98(-31)

Notes to Table 4: Specific power of each dust component in W/H atom resp.: total power, $4\pi \nu I_\nu(100)$, 3.3 μm feature power (the continuum being removed), $4\pi \Sigma_{IRAS} \nu I_\nu$ (see Pérault et al. 1989), power in the 5 to 1000 μm band and last column, power in the 10 to 120 μm (IRAS) band.

Table 5. IR emission of cirrus clouds

12	25	60	100	200	400	800	K(2.2)	L'(3.4)	X
9.37(-3)	5.71(-3)	1.27(-3)	3.34(-4)	4.41(-5)	2.99(-5)	5.87(-5)	3.66(-5)	5.48(-4)	3.0(-1)
5.31(-4)	6.18(-3)	3.17(-2)	1.77(-2)	4.65(-3)	2.75(-3)	1.77(-3)	9.06(-7)	1.51(-6)	3.0(-1)
0.00(0)	0.00(0)	5.78(-3)	5.83(-1)	2.38(-1)	3.78(-2)	4.62(-3)	0.00(0)	0.00(0)	3.0(-1)
9.91(-3)	1.19(-2)	3.87(-2)	6.01(-1)	2.43(-1)	4.07(-2)	6.51(-3)	3.66(-5)	5.48(-4)	3.0(-1)
1.56(-2)	9.52(-3)	2.11(-3)	5.56(-4)	7.37(-5)	5.87(-5)	1.88(-4)	6.11(-5)	9.14(-4)	5.0(-1)
8.86(-4)	1.03(-2)	5.28(-2)	2.95(-2)	7.89(-3)	4.62(-3)	2.47(-2)	1.51(-6)	2.52(-6)	5.0(-1)
0.00(0)	0.00(0)	1.69(-2)	8.85(-1)	2.99(-1)	4.40(-2)	0.00(0)	0.00(0)	0.00(0)	5.0(-1)
1.65(-2)	1.98(-2)	7.19(-2)	9.14(-1)	3.07(-1)	4.83(-2)	8.95(-2)	6.11(-5)	9.14(-4)	5.0(-1)
6.25(-2)	3.81(-2)	8.46(-3)	2.23(-3)	3.02(-4)	2.44(-4)	8.47(-4)	2.44(-4)	3.66(-3)	2.0(0)
3.54(-3)	4.13(-2)	2.12(-1)	1.17(-1)	3.25(-2)	1.87(-2)	1.01(-1)	6.04(-6)	1.01(-5)	2.0(0)
0.00(0)	0.00(0)	1.17(-1)	1.79(0)	5.19(-1)	7.19(-2)	0.00(0)	0.00(0)	0.00(0)	2.0(0)
6.60(-2)	7.93(-2)	3.47(-1)	2.04(0)	5.52(-1)	7.76(-2)	3.66(-1)	2.44(-4)	3.66(-3)	2.0(0)
9.37(-2)	5.71(-2)	1.27(-2)	3.34(-3)	4.62(-4)	3.66(-4)	1.25(-3)	3.66(-4)	5.47(-3)	3.0(0)
5.31(-3)	6.20(-2)	3.18(-1)	1.75(-1)	4.87(-2)	2.77(-2)	1.68(-2)	9.06(-6)	1.51(-5)	3.0(0)
0.00(0)	0.00(0)	1.75(-1)	2.89(0)	8.02(-1)	1.53(-1)	8.22(-2)	0.00(0)	0.00(0)	3.0(0)
9.90(-2)	1.19(-1)	5.09(-1)	3.06(0)	8.51(-1)	1.68(-1)	1.08(-1)	3.66(-4)	5.47(-3)	3.0(0)
1.56(-1)	9.51(-2)	2.11(-2)	5.56(-3)	7.94(-4)	6.25(-4)	8.47(-4)	6.10(-4)	9.12(-3)	5.0(0)
8.86(-3)	1.03(-1)	5.31(-1)	2.89(-1)	8.02(-2)	4.62(-2)	2.47(-2)	1.51(-5)	2.52(-5)	5.0(0)
0.00(0)	0.00(0)	2.89(-1)	4.12(0)	7.19(-1)	1.79(-1)	0.00(0)	0.00(0)	0.00(0)	5.0(0)
1.65(-1)	1.99(-1)	5.71(-1)	3.26(0)	6.51(-1)	1.06(0)	8.95(-2)	6.11(-4)	9.14(-3)	5.0(0)
3.12(-1)	1.90(-1)	4.23(-2)	1.11(-2)	1.69(-3)	1.25(-3)	3.78(-3)	1.22(-3)	1.82(-2)	2.0(1)
1.77(-2)	2.08(-1)	1.07(0)	1.21(0)	5.64(-1)	4.10(-2)	1.75(-1)	9.23(-5)	3.02(-5)	2.0(1)
0.00(0)	0.00(0)	3.01(0)	6.00(0)	9.04(-1)	9.77(-2)	0.00(0)	0.00(0)	0.00(0)	2.0(1)
3.30(-1)	3.99(-1)	4.12(0)	1.16(1)	6.57(0)	1.06(0)	1.40(-1)	1.22(-3)	1.83(-2)	2.0(1)
3.12(0)	1.90(0)	4.22(-1)	1.11(-1)	2.14(-2)	1.13(-2)	3.78(-3)	1.22(-2)	1.82(-1)	1.0(2)
1.78(-1)	2.23(0)	1.11(1)	4.12(0)	9.09(-1)	1.75(-1)	4.58(-1)	9.23(-4)	3.02(-4)	1.0(2)
1.80(-6)	1.36(-3)	3.01(0)	1.70(1)	1.79(0)	1.68(-1)	0.00(0)	0.00(0)	0.00(0)	1.0(2)
3.30(0)	4.12(0)	6.63(1)	8.26(1)	2.11(1)	3.47(-1)	1.40(0)	1.22(-2)	1.83(-1)	1.0(2)
3.13(1)	1.89(1)	4.17(0)	1.11(0)	2.08(-1)	5.06(-2)	1.05(-2)	1.22(-1)	1.83(-1)	1.0(3)
1.88(0)	3.22(1)	1.03(2)	6.71(1)	1.63(1)	2.78(0)	4.58(-1)	9.25(-5)	3.03(-3)	1.0(3)
3.81(-2)	8.33(1)	4.71(2)	2.87(2)	3.79(1)	3.21(0)	2.77(-1)	0.00(0)	0.00(0)	1.0(3)
3.32(1)	5.77(2)	5.44(1)	3.55(2)	6.04(1)	7.46(-1)	1.22(-1)	1.22(-1)	1.83(-1)	1.0(3)

Note to Table 5: This table and the following ones are organised as Table 3 (first half); see appendix B for details. The infrared emission of interstellar dust is calculated for different values of the ISRF intensity defined by X scaled at 1 for the LISRF (Pérault et al. 1989). For X = 1, refer to Table 3.

4. Comparison with observations

The parameters of the dust model given in §3.5 were optimised in order to reproduce the IR spectrum of cirrus HI emission in the Solar Neighborhood. In this section we compare model calculations with observations of the extinction curve and emission of dust in various physical environments in order to test the ability of the model to reproduce data over a wide range of conditions (radiation field variations). This comparison also aims at studying the composition of dust, in particular the abundance of small particles, in different components of the IS medium.

The model was used to compute the IR spectrum of each dust component including big grains, VSGs and PAHs embedded in radiation fields of different intensity and spectrum, enhancement in UV and different levels of attenuation by dust. The results of these calculations are presented in Tables 5 to 9 (see Appendix B for explanations and detailed hypotheses) and in Figures 7 to 11.

The presentation of the results and the discussion which follows are organised according to the type of environment they apply to (in order of increasing radiation field) and the data which exist for confrontation. The Tables may be used more generally to compute the emission of interstellar dust in different radiation fields for any proportions of the three basic components of the model.

4.1. Dark clouds

Figure 7 shows IR colours for various radiation fields that are relevant to dark clouds. To discuss the IR emission of dust in molecular clouds not heated by massive stars, we have to consider variations of the ISRF due to dust extinction (circles, using the extinction curve of Fig. 2) or related to the intrinsic

Table 6. IR emission of dark clouds

12	25	60	100	200	400	800	K(2.2)	L'(3.4)	Av
6.71(-3)	5.63(-3)	1.44(-3)	3.93(-4)	5.47(-5)	1.27(-4)	3.00(-4)	1.19(-5)	2.03(-4)	1.0(0)
4.46(-4)	5.83(-3)	3.68(-2)	4.88(-2)	2.66(-2)	8.62(-3)	5.77(-3)	1.36(-8)	4.70(-7)	1.0(0)
0.00(0)	6.05(-9)	1.63(-2)	2.81(-1)	8.84(-1)	2.99(-1)	4.40(-2)	0.00(0)	0.00(0)	1.0(0)
7.16(-3)	1.15(-2)	5.45(-2)	3.30(-1)	9.10(-1)	3.08(-1)	5.01(-2)	1.19(-5)	2.04(-4)	1.0(0)
2.46(-3)	2.49(-3)	6.83(-4)	1.90(-4)	2.76(-5)	1.23(-4)	2.99(-4)	2.20(-6)	4.12(-5)	2.0(0)
1.71(-4)	2.50(-3)	1.85(-2)	2.69(-2)	1.60(-2)	6.03(-3)	5.26(-3)	2.93(-9)	1.04(-7)	2.0(0)
0.00(0)	0.00(0)	5.70(-3)	1.34(-1)	5.93(-1)	2.41(-1)	3.81(-2)	0.00(0)	0.00(0)	2.0(0)
2.63(-3)	4.99(-3)	2.49(-2)	1.61(-1)	6.09(-1)	2.47(-1)	4.37(-2)	2.20(-6)	4.14(-5)	2.0(0)
1.11(-3)	1.26(-3)	3.62(-4)	1.02(-4)	1.57(-5)	1.20(-4)	2.97(-4)	5.38(-7)	1.09(-5)	3.0(0)
8.66(-5)	1.38(-3)	1.13(-2)	1.74(-2)	1.09(-2)	3.99(-3)	5.00(-3)	0.00(0)	2.89(-8)	3.0(0)
0.00(0)	0.00(0)	2.36(-3)	7.18(-2)	4.21(-1)	2.01(-1)	3.38(-2)	0.00(0)	0.00(0)	3.0(0)
1.19(-3)	2.64(-3)	1.40(-2)	8.93(-2)	4.32(-1)	2.05(-1)	3.91(-2)	5.39(-7)	1.09(-5)	3.0(0)
5.50(-4)	6.87(-4)	1.86(-4)	5.80(-5)	8.86(-6)	1.17(-4)	2.96(-4)	1.58(-7)	3.41(-6)	4.0(0)
5.15(-5)	8.72(-4)	7.58(-3)	1.22(-2)	7.97(-3)	3.49(-3)	4.84(-3)	0.00(0)	1.02(-8)	4.0(0)
0.00(0)	0.00(0)	1.08(-3)	4.11(-2)	3.09(-1)	1.70(-1)	3.04(-2)	0.00(0)	0.00(0)	4.0(0)
6.02(-4)	1.56(-3)	8.86(-3)	5.34(-2)	3.17(-1)	1.74(-1)	3.55(-2)	1.59(-7)	3.42(-6)	4.0(0)
2.92(-4)	3.91(-4)	1.06(-4)	3.43(-5)	5.00(-6)	1.14(-4)	2.94(-4)	5.35(-8)	1.22(-6)	5.0(0)
3.36(-5)	5.95(-4)	5.41(-3)	9.01(-3)	6.07(-3)	2.76(-3)	4.72(-3)	0.00(0)	4.41(-9)	5.0(0)
0.00(0)	0.00(0)	5.31(-4)	2.47(-2)	2.33(-1)	1.47(-1)	2.76(-2)	0.00(0)	0.00(0)	5.0(0)
3.25(-4)	9.87(-4)	6.06(-3)	3.38(-2)	2.39(-1)	1.50(-1)	3.26(-2)	5.36(-8)	1.23(-6)	5.0(0)

Note to Table 6: To estimate IR emission from dark clouds, we assume that the light propagates in only one direction and perpendicular to an infinite plane-parallel slab of optical thickness Av for which the scattering is strongly forward (i.e. the rays stay perpendicular to the slab); mathematically we simply multiply the LISRF by $e^{-\tau}$ where τ is the optical thickness by dust absorption at a given wavelength and for a given extinction Av, assuming the standard extinction curve as modeled in Fig. 2. More realistic assumptions are made by Bernard et al. (1990). The LISRF values correspond to Av = 0.

inhomogeneity of the UV part of the ISRF (crosses) which is due to a small number of stars unevenly distributed in the Galaxy. In Fig. 7, results obtained for a global scaling of the ISRF over the whole spectrum are also plotted (plus signs). Such global variations of the ISRF are relevant to discuss colours of clouds at different locations in a galaxy (see §4.2).

IRAS images of nearby molecular clouds show that the 12 and 25 μm emission is not simply related with the distribution of the 100 μm emission and/or that of large grains as traced by the visible extinction Av obtained from star counts. For clouds in Chameleon and Taurus, Boulanger et al. (1990) have measured colour ratios $R_{14} = I_\nu(12\,\mu m)/I_\nu(100\,\mu m)$ in the range 0.01 to 0.2. Fig. 7a shows that values of R_{14} significantly larger than the average value for cirrus in the Solar Neighbourhood of $\simeq 0.04$ are obtained in the model only for very weak radiation fields for which the emission from big grains is shifted to submillimetre wavelengths. For such values the model predicts a 100 μm emission per H atom much smaller than the values derived from the comparison of 100 μm emission and Av which gives typically $I_\nu(100\,\mu m)/N_H$ of 0.3 to 0.6 MJy/sr/(10^{20} H cm^{-2}) (Boulanger 1989). Furthermore, global variations of the ISRF over the whole spectrum are unrealistic within a complex of dark clouds. A more realistic variation of the ISRF, the one due to extinction by dust (circles in Fig. 7), reduces the R_{14} colour by a factor 2 to 4. Values of R_{14} as low as the observed ones (0.01)

are only obtained for the extreme case where the radiation field has the standard intensity in the visible and near-IR but very few UV photons. However, for the more plausible case where the UV radiation field is a factor 2 weaker than in the LISRF, the colour reduction is only marginal (0.04 to 0.03). Our calculations therefore support the conclusion of Boulanger et al. (1990) that colour variations in molecular clouds do not mainly result from variations in the radiation field but trace the abundance of small particles (PAHs and VSGs). In the IRAS images, the 25 μm is well correlated with the 12 μm emission. Unlike for the colours relative to the 100 μm intensity (R_{14}, R_{24} and R_{34}), the R_{12} colour is, within the measurement uncertainties, remarkably constant in dark clouds. This result indicates that the VSGs which make more than half of the emission in the 25 μm band must follow the abundance variation of PAHs. In this case of correlated variations of PAHs and VSGs, the model predicts that R_{34} should follow the variations of both R_{14} and R_{24}. However, this is not observed in some clouds: part of the scatter in R_{34} could be due to variation in the equilibrium temperature of BGs related to the growth of mantles.

Variations in the abundance of small particles indicated by colour changes must be related to changes observed in the extinction curve in molecular clouds (Massa and Savage 1989). The model may be used to predict the changes of the extinction curve in amplitude and shape which should result

Table 7. IR emission of cirrus clouds in different UV fields

12	25	60	100	200	400	800	K(2.2)	L'(3.4)	X_{UV}
7.67(-3)	8.02(-3)	2.20(-3)	6.13(-4)	8.53(-5)	1.30(-4)	2.99(-4)	2.31(-6)	5.61(-5)	-1.0(0)
3.85(-4)	5.72(-3)	4.28(-2)	6.08(-2)	3.47(-2)	1.07(-2)	6.13(-3)	2.63(-9)	1.03(-7)	-1.0(0)
0.00(0)	3.13(-8)	3.26(-2)	4.59(-1)	1.15(0)	3.46(-1)	4.87(-2)	0.00(0)	0.00(0)	-1.0(0)
8.06(-3)	1.37(-2)	7.76(-2)	5.20(-1)	1.19(0)	3.57(-1)	5.51(-2)	2.32(-6)	5.62(-5)	-1.0(0)
1.95(-2)	1.35(-2)	3.20(-3)	8.57(-4)	1.47(-4)	1.81(-4)	3.07(-4)	6.22(-5)	9.41(-4)	-5.0(-1)
1.08(-3)	1.32(-2)	7.43(-2)	4.66(-2)	1.88(-2)	1.34(-2)	6.70(-3)	4.75(-8)	1.56(-6)	-5.0(-1)
0.00(0)	8.85(-8)	4.81(-2)	5.99(-1)	1.34(0)	3.74(-1)	5.13(-2)	0.00(0)	0.00(0)	-5.0(-1)
2.05(-2)	2.67(-2)	1.26(-1)	6.91(-1)	1.37(0)	3.87(-1)	5.84(-2)	6.22(-5)	9.42(-4)	-5.0(-1)
4.30(-2)	2.45(-2)	5.26(-3)	1.37(-3)	1.81(-4)	2.14(-4)	4.39(-4)	1.82(-4)	2.71(-3)	5.0(-1)
2.46(-3)	2.81(-2)	1.37(-1)	1.53(-1)	7.10(-2)	1.88(-2)	8.32(-3)	1.37(-7)	4.48(-6)	5.0(-1)
0.00(0)	1.37(-7)	8.68(-2)	8.95(-1)	1.63(0)	4.19(-1)	5.56(-2)	0.00(0)	0.00(0)	5.0(-1)
4.55(-2)	5.26(-2)	2.29(-1)	1.05(0)	1.70(0)	4.38(-1)	6.36(-2)	1.82(-4)	2.71(-3)	5.0(-1)
5.48(-2)	3.01(-2)	6.29(-3)	1.62(-3)	1.51(-4)	1.60(-4)	3.09(-4)	2.42(-4)	3.59(-3)	1.0(0)
3.16(-3)	3.55(-2)	1.69(-1)	1.84(-1)	8.32(-2)	2.67(-2)	9.11(-3)	2.72(-7)	5.93(-6)	1.0(0)
0.00(0)	1.69(-7)	8.01(-2)	1.05(0)	1.77(0)	4.74(-1)	5.75(-2)	0.00(0)	0.00(0)	1.0(0)
5.80(-2)	6.56(-2)	2.85(-1)	1.23(0)	1.86(0)	4.61(-1)	6.59(-2)	2.42(-4)	3.60(-3)	1.0(0)
7.84(-2)	4.11(-2)	8.35(-3)	2.14(-3)	1.60(-4)	1.68(-4)	3.62(-4)	3.62(-4)	5.36(-3)	2.0(0)
4.54(-3)	5.04(-2)	2.32(-1)	2.45(-1)	1.07(-1)	3.20(-2)	1.01(-2)	3.61(-7)	8.85(-6)	2.0(0)
0.00(0)	2.15(-7)	1.61(-1)	2.03(0)	2.67(-2)	4.74(-1)	6.07(-2)	0.00(0)	0.00(0)	2.0(0)
8.29(-2)	9.15(-2)	4.01(-1)	1.61(0)	2.14(0)	5.01(-1)	7.01(-2)	3.62(-4)	5.37(-3)	2.0(0)
1.02(-1)	5.21(-2)	1.04(-2)	2.65(-3)	2.79(-4)	1.77(-4)	3.11(-4)	4.82(-4)	7.13(-3)	3.0(0)
5.93(-3)	6.53(-2)	2.94(-1)	3.06(-1)	1.32(-1)	3.73(-2)	1.10(-2)	3.61(-7)	1.18(-5)	3.0(0)
0.00(0)	2.94(-7)	2.15(-1)	1.68(0)	2.27(0)	5.04(-1)	6.34(-2)	0.00(0)	0.00(0)	3.0(0)
1.08(-1)	1.17(-1)	5.25(-1)	1.99(0)	2.40(0)	5.37(-1)	7.38(-2)	4.82(-4)	7.15(-3)	3.0(0)
1.25(-1)	6.31(-2)	1.25(-2)	3.16(-3)	3.44(-4)	1.68(-4)	3.10(-4)	6.01(-4)	8.90(-3)	4.0(0)
7.31(-3)	8.02(-2)	3.57(-1)	3.68(-1)	1.56(-1)	3.20(-2)	1.01(-2)	4.51(-7)	1.47(-5)	4.0(0)
0.00(0)	3.57(-7)	2.85(-1)	2.01(0)	2.48(0)	5.31(-1)	6.58(-2)	0.00(0)	0.00(0)	4.0(0)
1.33(-1)	1.43(-1)	6.55(-1)	2.38(0)	2.64(0)	5.69(-1)	7.72(-2)	6.02(-4)	8.92(-3)	4.0(0)
1.49(-1)	7.42(-2)	1.45(-2)	3.67(-3)	4.75(-4)	1.86(-4)	3.12(-4)	7.21(-4)	1.07(-2)	5.0(0)
8.70(-3)	9.52(-2)	4.20(-1)	4.29(-1)	1.80(-1)	4.25(-2)	1.20(-2)	5.41(-7)	1.76(-5)	5.0(0)
0.00(0)	1.50(-5)	3.55(-1)	2.33(0)	2.69(0)	5.56(-1)	6.80(-2)	0.00(0)	0.00(0)	5.0(0)
1.58(-1)	1.69(-1)	7.90(-1)	2.76(0)	2.87(0)	5.99(-1)	8.03(-2)	7.22(-4)	1.07(-2)	5.0(0)

Note to Table 7: Here one has added to the LISRF a fraction X_{UV} of its UV portion ($\lambda \le 300$ nm). Hence $X_{UV} = 0$ corresponds to the LISRF (Table 3) and $X_{UV} = -1$ represents the LISRF without any UV photons at all.

from the change in dust composition implied by the colour variations: Fig. 8 shows some examples of modified extinction curves. For the range of R_{14} colours observed in nearby clouds the extinction in the far-UV, for $A_V = 1$ will vary from 2.6 to 15 magnitudes at 100 nm, the standard value being 4.7. The correlation between the UV extinction curve and the R_{14} can be tested by measuring the UV extinction curve towards stars located behind regions of high and low R_{14}. Such observations will also provide an empirical measurement of the contribution of small particles to the extinction curve (Jenniskens and Désert 1990).

Finally, one can note in Fig. 7d that the 200 to 100 μm ratio is remarkably related to the emission at 100 μm per hydrogen atom, almost in an independent way from the heating radiation field. The reason is that one is dominated by one grain species (BGs). Hence the 200 to 100 μm ratio can be used as a dust "thermometer" with much more reliability than the 60-to-100 μm ratio which is plagued by VSGs emission. *COBE* and *ISO* satellites will soon shed some new light on this topic.

4.2. Cirrus emission

In Fig. 9, we have plotted the R_{34} 60 μm colour against the 100 μm emission normalised to the HI column density. The model emission (continuous line) is compared with cirrus emission (dashed line) in the outer Galaxy, the Solar Neighbourhood, and the molecular ring. Figure 9 also shows radial profiles across the two nearby galaxies M31 and M33. In M31, the present star formation rate is low and most of the IR emission is thought to come from cirrus (Walterbos and Schwering 1987). For M33 the situation is not

228

Table 8. IR emission of reflection nebulae

12	25	60	100	200	400	800	K(2.2)	L'(3.4)	X_B3
1.39(-1)	9.30(-2)	2.05(-2)	5.35(-3)	7.00(-4)	9.28(-5)	2.77(-5)	1.90(-2)	5.89(-3)	3.0(-3)
1.32(-2)	1.43(-1)	6.21(-1)	2.55(-1)	5.18(-2)	6.54(-3)	1.14(-4)	5.17(-2)	1.71(-2)	3.0(-3)
0.00(0)	5.97(-5)	3.49(0)	3.32(0)	3.77(-1)	8.52(-2)	2.61(-2)	0.00(0)	0.00(0)	3.0(-3)
1.52(-1)	2.36(-1)	4.11(0)	3.57(0)	4.30(-1)	9.51(-2)	5.85(-2)	1.78(-2)	1.78(-2)	3.0(-3)
3.95(-1)	2.56(-1)	5.52(-2)	1.43(-2)	1.86(-3)	2.46(-4)	5.01(-5)	5.17(-2)	1.71(-2)	1.0(-2)
3.99(-2)	4.33(-1)	1.83(0)	1.77(0)	6.91(-1)	1.51(-1)	2.77(-2)	2.48(-4)	8.47(-5)	1.0(-2)
0.00(0)	1.81(-3)	9.74(0)	9.74(0)	8.73(-1)	1.80(-1)	2.64(-1)	0.00(0)	0.00(0)	1.0(-2)
4.35(-1)	6.91(-1)	1.15(1)	1.15(1)	1.43(0)	3.32(-1)	9.51(-2)	5.85(-2)	1.78(-2)	1.0(-2)
1.13(0)	7.21(-1)	1.54(-1)	3.98(-2)	5.18(-3)	6.83(-4)	1.14(-4)	1.71(-1)	5.17(-2)	3.0(-2)
1.16(-1)	1.28(0)	5.29(0)	4.92(0)	1.80(0)	3.77(-1)	6.78(-2)	2.48(-4)	8.47(-5)	3.0(-2)
4.64(-9)	3.71(-2)	2.48(1)	2.48(1)	1.20(0)	9.51(-2)	0.00(0)	0.00(0)	0.00(0)	3.0(-2)
1.25(0)	2.04(0)	2.98(1)	2.98(1)	1.12(1)	1.58(0)	1.90(-1)	1.78(-1)	5.19(-2)	3.0(-2)
3.70(0)	2.35(0)	5.00(-1)	1.29(-1)	1.68(-2)	2.21(-3)	3.37(-4)	5.66(-1)	1.71(-1)	1.0(-1)
3.86(-1)	4.49(0)	1.74(1)	4.72(0)	9.16(-1)	1.59(-1)	2.52(-5)	8.20(-4)	3.0(-1)	1.0(-1)
3.06(-6)	7.20(-1)	6.25(1)	1.56(1)	1.68(0)	1.60(-1)	0.00(0)	0.00(0)	0.00(0)	1.0(-1)
4.08(0)	7.56(0)	7.74(1)	2.04(1)	2.60(0)	3.19(-1)	1.71(-1)	5.66(-1)	1.71(-1)	1.0(-1)
1.10(1)	6.99(0)	1.49(0)	3.82(-1)	4.97(-2)	6.54(-3)	9.71(-4)	1.70(0)	5.10(-1)	3.0(-1)
1.18(0)	1.52(1)	5.03(1)	3.64(1)	9.79(0)	1.73(0)	2.88(-1)	2.52(-5)	8.20(-5)	3.0(-1)
4.41(-4)	7.56(0)	1.41(2)	6.25(1)	2.25(0)	1.60(0)	2.04(-1)	0.00(0)	0.00(0)	3.0(-1)
1.22(1)	2.98(1)	1.93(2)	1.67(2)	3.34(1)	3.99(0)	4.93(-1)	1.70(0)	5.13(-1)	3.0(-1)
3.67(1)	2.31(1)	4.89(0)	1.26(0)	1.63(-1)	2.15(-2)	3.15(-3)	5.67(0)	1.70(0)	1.0(0)
4.18(0)	6.40(1)	1.47(2)	8.45(1)	1.85(1)	2.99(0)	4.77(-1)	2.52(-4)	8.20(-3)	1.0(0)
4.01(-2)	6.86(1)	4.04(2)	2.57(2)	3.03(1)	2.64(0)	0.00(0)	0.00(0)	0.00(0)	1.0(0)
4.09(1)	1.56(2)	5.56(2)	3.43(2)	5.40(1)	6.04(0)	7.44(-1)	5.67(0)	1.71(0)	1.0(0)
1.10(2)	6.86(1)	1.43(1)	3.65(0)	4.72(-1)	6.19(-2)	9.06(-3)	1.71(1)	5.13(0)	3.0(0)
1.52(1)	2.45(2)	3.45(2)	1.59(2)	2.95(1)	4.46(0)	6.92(-1)	7.61(-4)	2.47(-2)	3.0(0)
1.21(0)	3.79(2)	9.16(2)	4.37(2)	4.91(1)	3.92(0)	3.30(-1)	0.00(0)	0.00(0)	3.0(0)
1.26(2)	6.93(2)	1.27(3)	5.99(2)	7.91(1)	8.44(1)	1.03(0)	1.71(1)	5.15(0)	3.0(0)

Note to Table 8: The radiation field is the sum of the LISRF and X_{B3} times the spectrum of a B3 star at a distance of 0.15 pc. The B3 star is assumed to emit like a blackbody of effective temperature $T_{eff} = 2\times10^4$ K with a luminosity $L = 8\times10^3 L_{\odot}$ and with a cutoff for frequencies above the Lyman continuum. Hence the IR emission of dust at 1.5 pc from the star corresponds to $X_{B3} = 10^{-2}$. The energy density is 210 eV/cm³ at 0.15 pc from the star. PAHs are assumed to be ionized.

so clear cut. About half of the emission is thought to come from cirrus, the other half comes from HII regions and their vicinity (Rice et al. 1989). In these two galaxies and the Milky Way, the 60 to 100 μm colour (R_{34}) shows little variation with the intensity of the radiation field as measured by the 100 μm emissivity per hydrogen atom [metallicity effects may however influence this measure]. This result has been qualitatively explained by the contribution of small particles to the 60 μm emission (Draine and Anderson 1985). Fig. 9 shows that our model quantitatively reproduces the small variations of R_{34} across the Galaxy and M31 - see §3.4 for the implied change of BG emissivities. The colours in M33 are slightly higher than predicted, which probably results from the contribution of HII regions mainly to the 60 μm band. For the LISRF, about 2/3 of the 60 μm emission comes from VSGs (compare dotted curve and continuous curve in Fig. 9).

4.3. Reflection nebulae

Figure 10 compares the IR observations of the Pleiades (Castelaz et al. 1987, see also Cox and Leene 1986 who also reduced the Pleiades IRAS data) with the model computed using the radiation field of a B3 star. It shows that the observed colour R_{14} and the "energy ratio" $\Gamma_1 = \nu I_\nu(12)/(\nu I_\nu(60) + \nu I_\nu(100))$ rise when R_{34} increases (full triangles) i.e. when approaching the exciting star 23 Tau (spectral type B6). A similar but weaker effect is seen with R_{24} and Γ_2. The most straightforward explanation is that the abundance of PAH and VSG in the gas immediately surrounding the star is larger by about a factor of 2 than the average cirrus value. Large enhancements of the PAHs abundance at the edges of molecular clouds have been observed (see §4.1). Indeed, one can remark that the Pleiades stars also lie close to a molecular cloud (c.f. CO map by Ungerechts and Thaddeus 1987). They

Table 9. IR emission near an O5 star

12	25	60	100	200	400	800	K(2.2)	L(3.4)	X$_{O5}$
4.32(-2)	3.16(-2)	7.18(-3)	1.87(-3)	2.46(-4)	1.68(-4)	3.24(-4)	5.59(-3)	1.62(-3)	1.0(-4)
2.59(-3)	2.87(-2)	1.34(-1)	1.46(-1)	6.63(-2)	1.77(-2)	7.77(-3)	1.87(-7)	5.83(-6)	1.0(-4)
0.00(0)	5.29(-7)	9.14(-2)	1.66(0)	4.23(-1)	5.60(-2)	0.00(0)	0.00(0)	0.00(0)	1.0(-4)
0.00(0)	6.03(-2)	2.32(-1)	1.07(0)	1.73(0)	4.41(-1)	6.41(-2)	5.59(-3)	1.62(-3)	1.0(-4)
7.17(-2)	4.89(-2)	1.07(-2)	2.76(-3)	3.60(-4)	1.83(-4)	3.26(-4)	1.25(-2)	3.25(-3)	3.0(-4)
4.21(-3)	4.47(-2)	1.89(-1)	1.95(-1)	8.38(-2)	2.14(-2)	8.42(-3)	3.76(-7)	1.14(-5)	3.0(-4)
0.00(0)	2.09(-6)	1.51(-1)	1.97(0)	4.66(-1)	5.99(-2)	0.00(0)	0.00(0)	0.00(0)	3.0(-4)
7.60(-2)	3.51(-1)	1.49(0)	2.06(0)	4.87(-1)	6.87(-2)	1.25(-2)	3.26(-3)		3.0(-4)
1.72(-1)	1.10(-1)	2.30(-2)	5.87(-3)	7.58(-4)	2.35(-4)	3.33(-4)	3.69(-2)	8.94(-3)	1.0(-3)
9.89(-3)	1.01(-1)	3.82(-1)	3.64(-1)	1.45(-1)	3.41(-2)	1.07(-2)	1.04(-6)	3.09(-5)	1.0(-3)
0.00(0)	2.95(-5)	4.34(-1)	2.64(0)	5.75(-1)	6.97(-2)	0.00(0)	0.00(0)	0.00(0)	1.0(-3)
9.36(-2)	3.51(-1)	1.49(0)	2.06(0)	4.87(-1)	6.87(-2)	3.69(-2)	8.98(-3)		1.0(-3)
4.57(-1)	2.83(-1)	5.82(-2)	1.47(-2)	1.90(-3)	3.84(-4)	3.55(-4)	1.07(-1)	2.52(-2)	3.0(-3)
2.61(-2)	2.61(-1)	9.35(-1)	8.46(-1)	3.16(-1)	6.98(-2)	1.70(-2)	2.93(-6)	8.66(-5)	3.0(-3)
0.00(0)	6.10(-4)	1.61(0)	6.45(0)	7.59(-1)	8.55(-2)	0.00(0)	0.00(0)	0.00(0)	3.0(-3)
1.82(-1)	2.10(-1)	8.40(-1)	3.01(0)	2.99(0)	6.09(-1)	8.07(-2)	3.69(-2)	8.98(-3)	3.0(-3)
1.46(0)	8.88(-1)	1.81(-1)	4.58(-2)	5.87(-3)	9.04(-4)	6.46(-4)	3.50(-1)	8.22(-2)	1.0(-2)
8.30(-2)	8.29(-1)	2.87(0)	8.85(-1)	1.86(-1)	8.48(-2)	9.48(-5)	2.82(-4)		1.0(-2)
1.43(-9)	1.71(-2)	7.43(0)	1.82(0)	1.07(0)	1.11(-1)	0.00(0)	0.00(0)	0.00(0)	1.0(-2)
1.54(0)	1.73(0)	8.40(-1)	8.81(0)	1.26(0)	1.49(-1)	3.50(-1)	8.25(-2)		1.0(-2)
4.31(0)	2.62(0)	5.33(-1)	1.34(-1)	1.72(-2)	2.39(-3)	6.46(-4)	1.05(0)	2.45(-1)	3.0(-2)
2.46(-1)	2.50(0)	8.39(0)	6.97(0)	2.31(0)	4.63(-1)	8.48(-2)	2.85(-5)	8.41(-4)	3.0(-2)
5.96(-7)	2.74(-1)	2.75(1)	1.02(1)	2.05(0)	1.10(0)	0.00(0)	0.00(0)	0.00(0)	3.0(-2)
4.55(0)	3.64(1)	5.09(1)	1.51(1)	1.93(0)	2.28(-1)	1.05(0)	2.46(-1)		3.0(-2)
1.43(1)	8.65(0)	1.76(0)	4.43(-1)	5.67(-2)	7.55(-3)	1.40(-3)	3.49(0)	8.15(-1)	1.0(-1)
8.24(-1)	8.87(0)	2.73(1)	2.05(1)	5.94(0)	1.10(0)	1.89(-1)	9.48(-5)	2.80(-3)	1.0(-1)
1.60(-4)	3.93(0)	9.86(1)	1.02(2)	2.05(1)	2.03(0)	0.00(0)	0.00(0)	0.00(0)	1.0(-1)
1.51(1)	2.15(1)	1.28(2)	2.65(1)	3.14(0)	3.78(-1)	3.49(0)	8.18(-1)		1.0(-1)
4.27(1)	2.58(1)	5.21(0)	1.31(0)	1.68(-1)	2.20(-2)	3.51(-3)	1.05(1)	2.45(0)	3.0(-1)
2.54(0)	3.03(1)	7.69(1)	4.92(1)	1.20(1)	2.04(0)	3.36(-1)	2.84(-4)	8.39(-3)	3.0(-1)
1.11(-2)	3.19(1)	2.71(2)	3.01(1)	2.69(0)	2.37(-1)	0.00(0)	0.00(0)	0.00(0)	3.0(-1)
4.53(1)	8.80(1)	3.53(2)	4.22(1)	4.75(0)	5.76(-1)	1.05(0)	2.45(0)		3.0(-1)
1.42(2)	8.47(1)	1.69(1)	4.21(0)	5.36(-1)	7.01(-2)	1.05(-2)	3.52(1)	8.18(0)	1.0(0)
9.31(0)	1.25(2)	2.15(2)	1.10(2)	2.22(1)	3.48(0)	5.49(-1)	9.50(-4)	2.80(-2)	1.0(0)
5.31(-1)	2.27(2)	6.99(2)	3.65(2)	4.38(1)	3.58(0)	3.05(-1)	0.00(0)	0.00(0)	1.0(0)
1.52(2)	4.37(2)	9.31(2)	4.79(2)	6.65(1)	7.13(0)	3.52(1)	8.21(0)		1.0(0)
4.20(2)	2.44(2)	4.70(1)	1.16(1)	1.46(0)	1.89(-1)	2.78(-2)	1.08(2)	2.47(1)	3.0(0)
3.62(1)	4.56(2)	4.81(2)	2.00(2)	3.48(1)	5.13(0)	7.89(-1)	2.87(-3)	8.47(-2)	3.0(0)
1.03(1)	1.05(3)	1.47(3)	5.92(2)	5.97(1)	4.58(0)	3.80(-1)	0.00(0)	0.00(0)	3.0(0)
4.67(2)	1.75(3)	1.99(3)	8.04(2)	9.60(1)	9.91(0)	1.20(0)	1.08(2)	2.48(1)	3.0(0)
1.35(3)	7.33(2)	1.30(2)	3.09(1)	3.80(0)	4.89(-1)	7.10(-2)	3.77(2)	8.40(1)	1.0(1)
2.16(2)	1.67(3)	1.00(3)	3.44(2)	5.26(1)	7.38(0)	1.11(0)	9.81(-3)	2.90(-1)	1.0(1)
1.64(2)	4.42(3)	2.96(3)	9.45(2)	8.19(1)	5.95(0)	4.82(-1)	3.30(-9)	1.61(-7)	1.0(1)
1.73(3)	6.83(3)	4.10(3)	1.32(3)	1.38(2)	1.38(1)	1.66(0)	3.77(2)	8.43(1)	1.0(1)

Note to Table 9: The radiation field is the sum of the LISRF and X$_{O5}$ times the spectrum of an O5 star at a distance of 1 pc. The spectrum of the O5 star is computed by starting from a blackbody of $T_{eff} = 4 \times 10^4$ K and $L = 8 \times 10^5\, L_\odot$ and converting the photons above the Lyman continuum limit into Lyman α photons. The energy density of the radiation field is 400 eV/cm^3 at 1pc from the star. PAHs are assumed to be ionized.
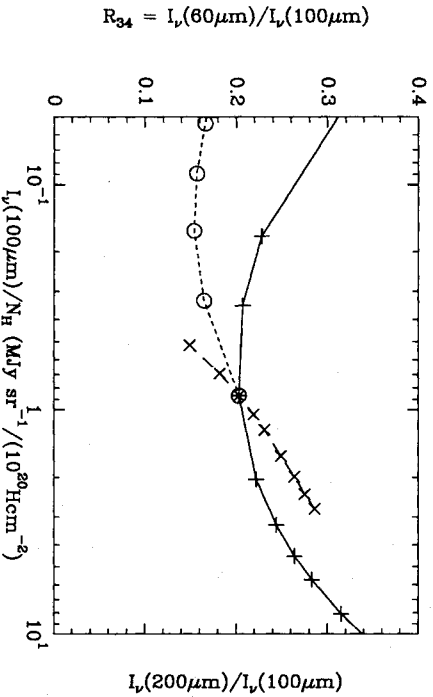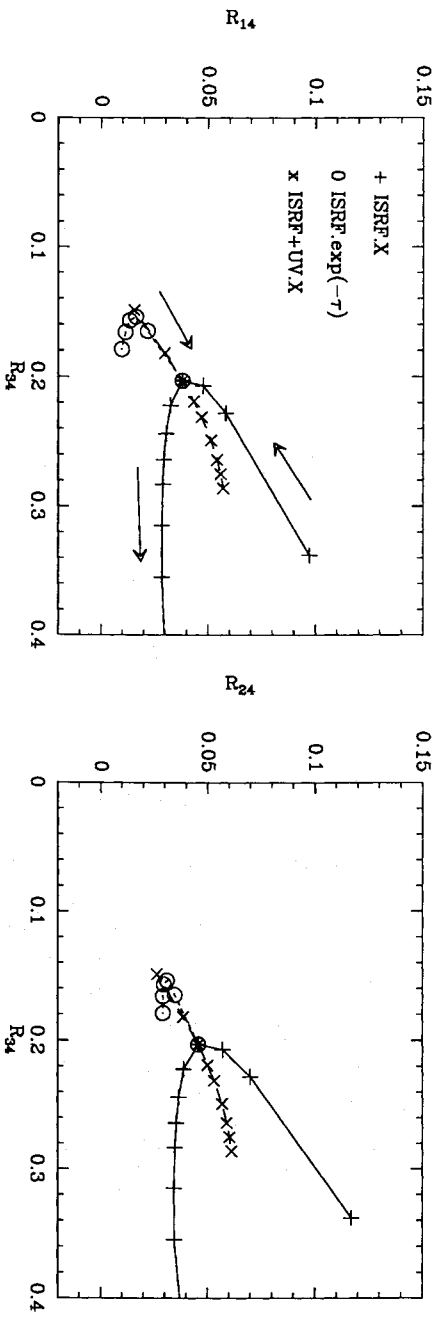
230

Fig. 7. Infrared colours of cirrus and dark clouds. Keeping the abundance of grains constant, the radiation field varies from one point to another. Variations are global for the plus signs, or concerning the UV ISRF only (crosses), or the ISRF is reduced by some extinction (circles). The signs correspond to the different entries in Table 3, 5, 6 and 7. The four IRAS bands are 1, 2, 3, and 4, corresponding to 12, 25, 60, 100μm resp. (e.g. $R_{14} = I_\nu(12\,\mu m)/I_\nu(100\,\mu m)$). All three curves go through the same point corresponding to the undisturbed LISRF. The radiation energy density increases monotonically with $I_\nu(100\,\mu m)/N_H$ and along the arrows. A similar diagram is discussed by Laureijs (1989) for Chlewicki and Laureijs (1988) dust model.
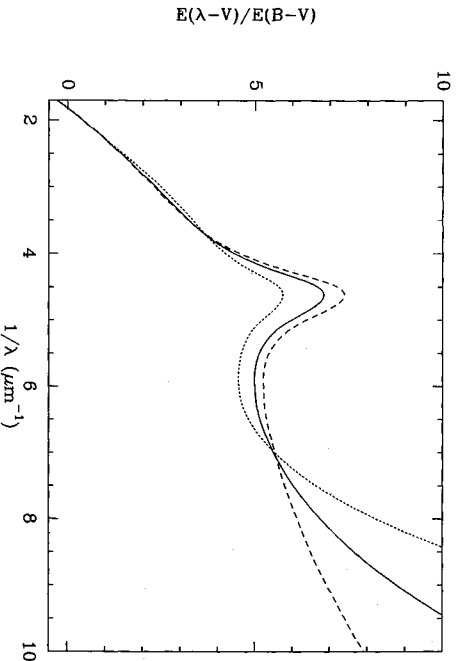
Fig. 8. UV Extinction curves normalised to E_{B-V} for three different PAH abundances: normal Y_{PAH} (cf. Table 2, solid curve), $Y_{PAH}/4$ (dashed curve) and $4Y_{PAH}$ (dotted curve). These abundances span the whole observed range in dark clouds as deduced from the R_{14} IR colour variations. Notice that, although VSG abundance is kept constant, the bump strength varies only because of the normalisation to E_{B-V} and the contribution by PAHs to the visible. On the other hand, only the low part of the extinction curve changes if VSG abundance varies (not shown here).

are best interpreted by the release of organic material from grain mantles exposed to UV radiation. There is competition between such a mechanism (which increases the abundance of PAHs and VSGs) and the destruction of PAHs by UV radiation field as discussed in next Section. The increase in the PAH abundance might be related to the fact that this reflection nebula is excited by a late B star. It could indicate that, in reflection nebulae, the ratio R_{14} would first increase going from A stars to late B stars and then decrease when going toward early B stars and O stars. This would account for the result of Sellgren (1989).

4.4. HII regions

Figure 11 shows the IR colour variations at different distances from an O5 star. For the chosen parameters, the radiation field energy density is about 200 eV cm⁻³ at 1 pc from the star. Observations are that of ξ Per (Boulanger et al. 1988 and Ryter, private communication). First, we see good agreements between the model and the observations at the three largest IRAS wavelengths: 25, 60, 100μm. In particular, one can notice that, in the model, R_{24} (the 25 to 100 μm flux ratio) has a plateau for low values of R_{34}, then rises for values of R_{34} larger than about 0.8. This behaviour has already been described by Boulanger
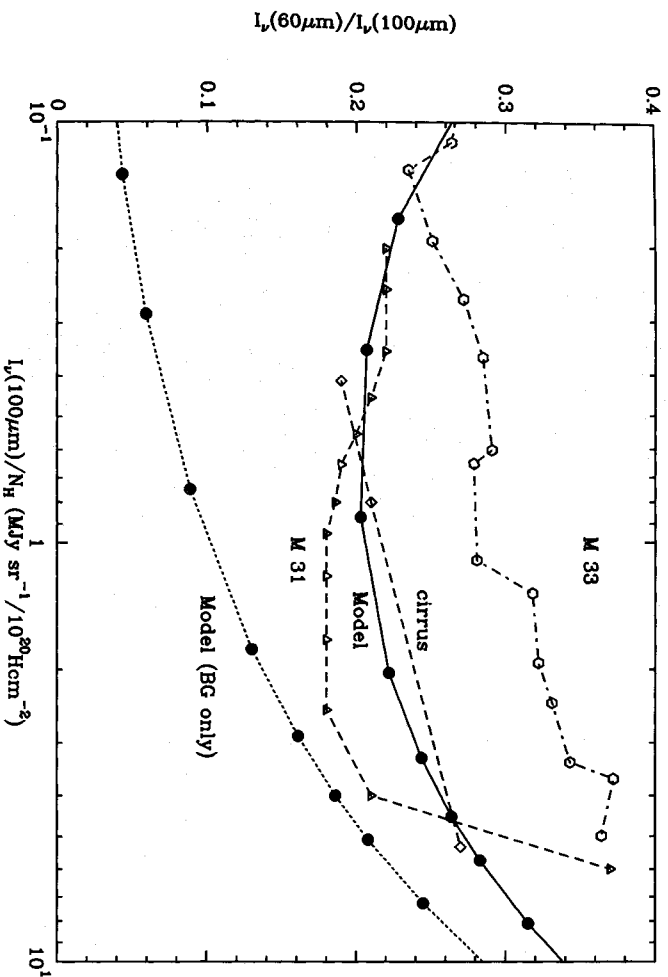
Fig. 9. Far IR colours of the interstellar medium. The model (total: continuous curve; BG only: dot continuous curve; BG only: dot curve) is compared to cirrus clouds (diamonds) in the outer galaxy, in the solar neighbourhood and in the molecular ring (Pérault et al. 1989), and to two nearby galaxies M 33 and M 31 (Wal-terbos and Schwering 1987). Metal-licity gradients have *not* been taken into account. They would shift the observation points on an horizontal line if metallicity varies globally without changing the dust composition. Note the increasing importance of VSGs at low radiation field (left part of the graphic) which are necessary in order to understand the far IR colours of inactive galaxies.
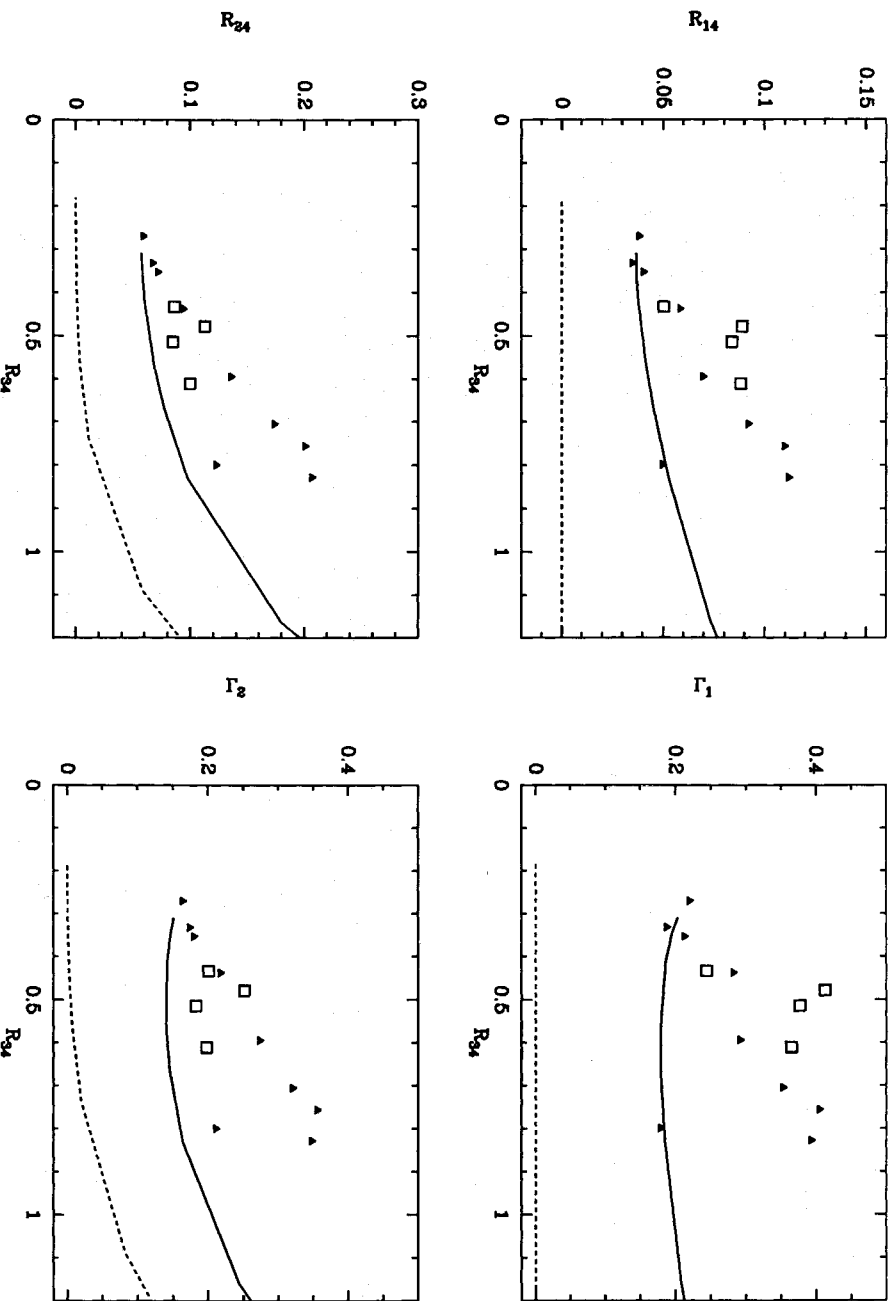
Fig. 10. Near IR colours of reflection nebulae. The model (total: continuous curve; BG only: dashed curve) predicts increasing colours when the dust is located nearer to the illuminating star (assumed here of B3 spectral type). Observations of the Pleiades with IRAS (Castelaz et al. 1987) are reported as triangles (a slice near 23 Tau) and squares (for the global colours of the clouds illuminated by the four stars. The model shows that the variables $\Gamma_1 = \nu I_\nu(12)/(\nu I_\nu(60) + \nu I_\nu(100))$ and Γ_2 (same for 25 μm band) are approximately independent of the distance to the star (in this range of far IR colour R_{34}). Notice that the Pleiades show an increase of the abundance of PAHs and/or VSGs of up to a factor two.
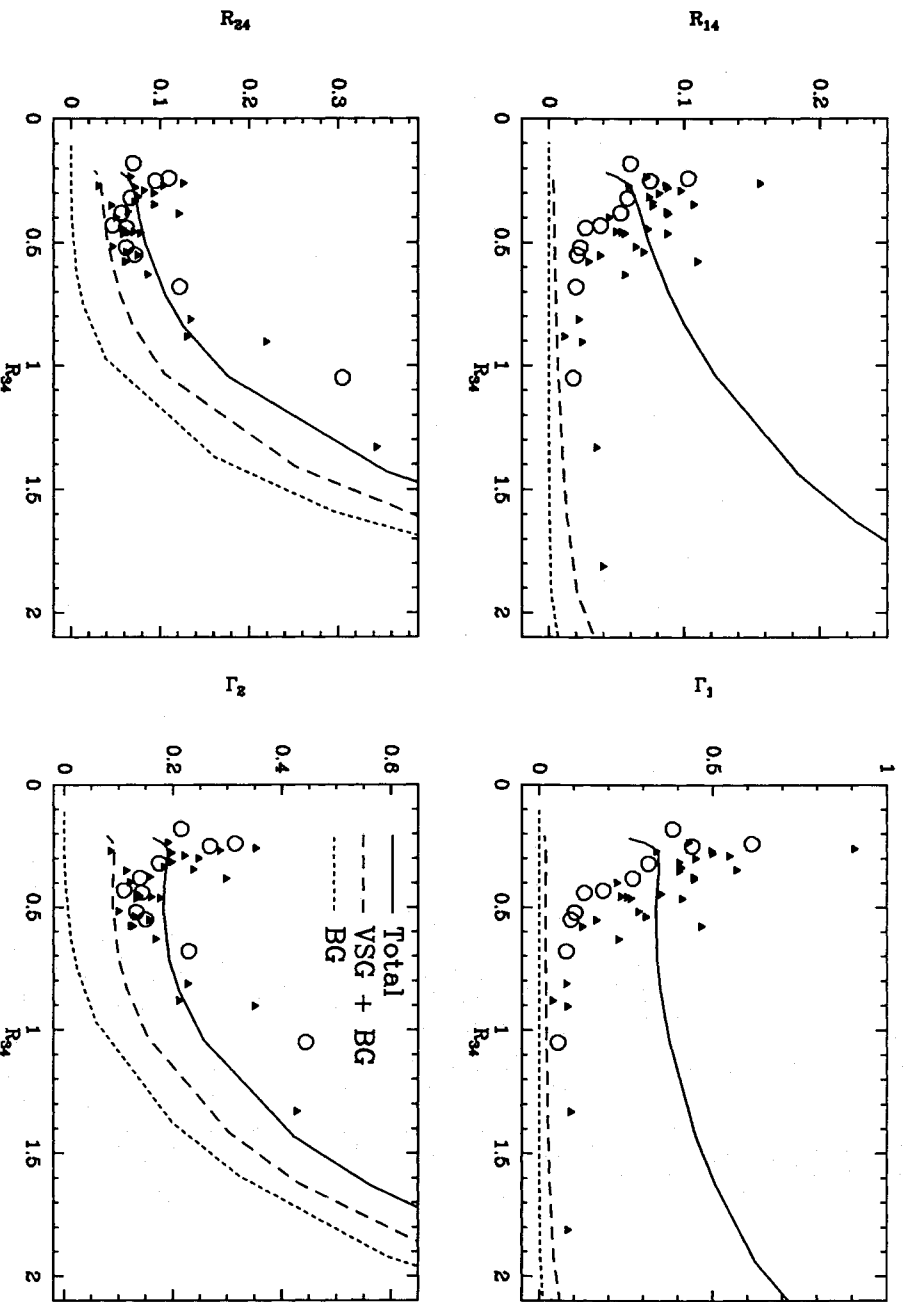
231

Fig. 11. Near IR colours of HII regions. The model (total: continuous curve; BG only: dashed curve) is compared with observations of the California Nebula (ξ Per) (Boulanger et al. 1988: circles; Ryter (private communication); triangles obtained from isolated filaments). Whereas PAHs, emitting at 12 μm, are absent when the radiation field is strong (ie. R_{34} large), VSGs do not seem to disappear and could even be overabundant. The large values of the near IR colours at low R_{34} could be due to: 1) an overabundance of both PAHs and VSGs; or 2) suppression (e.g. by some large extinction) of the ISRF that has been added to an O5 star radiation field.

et al. (1988) and is a consequence of the assumption of VSGs. One also notices the large values of R_{14} and R_{24} (about 0.06) compared with the "cirrus" medium values (0.04-0.05, Table 3) for the same $R_{34} \simeq 0.2$. This is due to the incident spectrum which, near an O star, is much stronger in UV photons than the LISRF, hence PAHs and VSGs are relatively more heated than BGs.

Secondly, the disagreement at 12 μm (see R_{14} in Figure 11a) between the dust model and the observations for $R_{34} \geq 0.5$ is emphasised here. Found by de Vries (1985), RPP and Boulanger et al. (1988), it seems to be a general feature of the interstellar dust in our Galaxy that in strong radiation field the 12 μm emitting particles (PAHs in our model) are absent i.e. probably destroyed. For example, for $R_{34} \simeq 1$, the abundance of PAHs is reduced by at least a factor of 10. As a strong argument for our assumption that PAHs are the carriers of the FUVnl extinction curve, the extinction curves of α Cam and ξ Per (Bless and Savage 1972) are relatively flat in the FUV. Caution should be applied however for the case of ζ Oph (Ryter, private communication) where it is known that the extinction mainly occurs in two molecular clumps along the line of sight and not near the star, hence its more normal extinction curve.

Thus, the dust model that has been fitted to the cirrus HII medium, is able to account for the IR colours of dust in the radiation field of nearby stars. The abundance of PAHs is however much reduced in strong radiation fields. On the other hand, there is no evidence for the destruction of VSGs in strong radiation fields as deduced from the observed R_{24} colours, after the contribution of PAHs to the 25 μm band has been subtracted (see dashed curves in Fig. 11). On the contrary, the data indicate that there may be an excess emission at 25 μm, compared with the model: it could either mean that there is an excess of VSGs close to the star or that BGs emissivities have to be modified. These conclusions are also reached by Cox, Deharveng and Leene (1990) from the study of the Rosette Nebula. It is known that dust is partly destroyed or processed in compact HII regions as shown by Chini, Krügel and Kreysa (1986). From these remarks, we deduce that the 25 μm emission is not completely due to PAHs: hence our assumption that half the emission in the 25 μm band comes from VSGs (Section 3.3.2).

The R_{12} colour is relatively constant for $R_{34} \leq 1$ in the model while the observations (e.g. Boulanger et al. 1988) show a decrease, i.e. an anticorrelation, which reflects the destruction of PAHs.

4.5. Consequences on PAH abundance and UV penetration in clouds

In HII regions associated with early B stars (e.g. σ Sco), the ratio Γ_1 has been shown to decrease to about 0.06 (see RPP) when the UV energy density reaches about 100 eV/cm³ or when R_{34} reaches about 2. This is interpreted as the result of the destruction of PAHs by UV photons and the abundance is then lower than the average cirrus value by a factor of 10. When R_{34} is only 0.7, there is no depletion observed when compared to the predicted values.

In the vicinity of O stars the same effect is found (Boulanger et al. 1988) but appears even earlier in terms of the temperature of big grains as measured by R_{34}. As can be seen in Figure 11, the observed Γ_1 becomes smaller than 0.1 for $R_{34} = 0.7$, implying in this case a depletion of PAHs by a factor 5. For $R_{34} = 1.8$, Γ_1 is lower than the prediction of the model by at least a factor 10, thus indicating a deficit of PAHs of that magnitude in comparison to the average cirrus value. This proves that the total intensity of the radiation field is less critical a factor than the presence of hard UV photons although it is difficult to give a more quantitative picture of this phenomenon.

The model predicts that the very efficient destruction of PAHs by hard UV photons leads to an extinction curve without FUVnl rise, which is observed in a few specific case where we know that the extinction is dominated by the UV illuminated material: σ Sco, θ Ori... The situation is less clear cut for VSGs assumed to produce the bump in the extinction curve. In any case, this mechanism of destruction of UV extinction by UV photons considerably modifies our view of the propagation of hard UV photons in galaxies, HII regions, photodissociation regions. When the energy density of hard UV photons (like those radiated by O stars) reaches 30 eV/cm³ (which leads to $R_{34} = 0.7$) the abundance of PAHs drops by about a factor of 5, and it drops by a factor of more than 10 when R_{34} reaches 2. This implies an extinction curve where the FUV extinction (100 nm) $\sigma_H = 1.2 \times 10^{-21}$ cm²/H instead of 2.35×10^{-21} for an average galactic extinction curve. Furthermore, at the same time, the albedo doubles from 0.28 to 0.56 which altogether means that the absorbing part of the extinction curve drops by a factor of 5. The FUV radiation propagates much more easily because of the increase of the mean free path and because the increased albedo helps considerably its propagation in a clumpy medium (Boissé 1990).

Table 9 (and the others too) reveals another feature. When the energy density increases, the peak of the BG emission shifts towards shorter wavelengths. In this case, one can note that at submillimetre wavelengths, the ratio of the VSG emission to the emission from BGs *increases* with wavelength. For example, at 200 μm the VSG to BG emission ratio reaches 10% at 10pc from the O5 star ($X_{O5} = 10^{-2}$) and is 50% at 1 pc. At 400 μm, the ratio is unity at 1pc. There are two reasons for this behaviour. The IR emission spectrum from VSGs compared with the spectrum from BGs (for an equal amount of absorbed energy) is wider because the VSG temperature fluctuates around its equilibrium temperature. Hence, the emission of VSGs can dominate that of BGs if BGs are hot enough and the emission of VSGs is larger or equal to the BG emissivity at submillimetre wavelengths. This effect is allowed in our model because the emissivity of carbonaceous VSGs has been assumed to decrease as λ^{-1} instead of $\simeq \lambda^{-2}$ for BGs (Seki and Yamamoto 1980) and therefore VSGs emissivity dominates in the submillimetre range (see Fig. 3). This has an important consequence when submillimetre and millimetre continuum measurements are used to derive a dust column density in the vicinity of stars. If a fraction of the submillimetre emission is dominated by VSGs (fluctuating in temperature) by a factor 2 or 3, then the derived column density could be overestimated by the same factor. The observed emissivities can be less steep than the BG emissivities. This might account for the discrepancies observed between the determination of column densities from continuum measurements and from molecular transitions (HCN, $C^{18}O$, NH_3...) as in S 106 (Mezger et al. 1987).

5. Main features of interstellar dust models

The dust model presented above has several broad characteristics that are listed below. It is likely that future dust models will possess some of these characteristics as well.

1) It is minimal in its number of distinct components of IS dust that are needed to account for various observations (§ 2): PAHs, VSGs and BGs generally coexist in the IS medium though locally, some large abundance variations are observed (see e.g. § 4.3). New observations or more detailed modeling of existing data may indicate that additional components are necessary. For example, the Magellanic Clouds have very peculiar extinction curves and IR spectra (see e.g. Lequeux 1989) that may require a new type of grain. This is however unlikely to affect much the IR emission of our Galaxy.

2) It is consistent with cosmic abundances of elements, especially C, O, Si, Mg. For the present model, the abundance of carbon in solids (relative to solar abundances) is about 8% for PAHs, 8% for VSGs and 25% in BGs (as estimated by Tielens and Allamandola 1987 for the latter) with a large uncertainty due to uncertain optical constants. The abundances of Si and Mg in solids are almost equal to the solar abundances.

3) The grain optical properties are inferred *both* from astronomical observations and from laboratory data on possible grain candidates, as was done by Draine and Lee (1984) in an earlier MRN-type dust model; the model was *not* built from an *ab initio* grain composition which was then fitted to the observations; rather, we have adapted the optical properties of likely candidates in order to be consistent with the average extinction curve and IR emission; so far, "astronomical" grains have proven to be different from any laboratory analogues. For example, PAHs are larger than laboratory PAHs and can be ionised and dehydrogenated; astronomical VSGs have a narrower 220nm bump than any existing carbon candidates; and astronomical BGs are a mixture of hydrocarbons and silicates for which data on optical properties are very scarce.

4) The model is far from unique at present, and it will have to be modified and/or completed as more observations and laboratory data are gathered. A lot of additional constraints could be obtained from the analysis of extreme FUV data ($x = \lambda^{-1} \geq 8 \mu m^{-1}$), IR spectroscopy of features, especially in low brightness sources with *ISO*, submillimetre data (e.g. from the *COBE* satellite) and paradoxically, visible and very NIR data e.g. the red luminescence, albedos and phase function of grains...

5) The model can be extended to include the cycling of IS grains through the molecular phase (see § 4.4) in which various ices can exist on BGs, smaller grains are accreted or coagulated, and PAH abundance is variable by an order of magnitude, in a manner similar to the cycling of dust proposed by Greenberg (1982, 1986), Seab (1987), and Boulanger et al. (1990).

233

234

6) The model should be useful to *both* the observers – several tables and figures are given to allow easy comparison of data – and the theoreticians – hints for the likely composition and optical properties of all the dust components have been made here.

7) Any future model is likely to require transiently heated small grains in order to explain a large variety of observations (see the review by Puget and Léger 1989). These grains – we argue – account for an appreciable part ($\simeq 40\%$) of the energy absorbed by dust.

Unavoidable consequences of the model are that 1) it allows disentangling excitation effects from abundance variations: for example, there is strong evidence for the destruction of the smallest particles (PAHs) in strong radiation fields and large abundance variations near molecular clouds, so far based only on photometric data because of low brightness; 2) there is a direct link between extinction curves and IR emission spectra – more work needs to be carried out to establish in more details which component of the extinction curve; 3) several issues of the model will not be settled until more laboratory data are gathered.

Acknowledgements. We wish to thank J. P. Bernard, P.Boissé, P. Cox, L. d'Hendecourt, T. Désert, J. M. Greenberg, A. Léger, J. Lequeux, M. Pérault and C. Ryter for many useful discussions. This work was done while one of us (F.-X. D.) held an N. R. C. Associateship at NASA Goddard Space Flight Center and then an external ESA Fellowship at the Laboratory Astrophysics, Huygens Laboratorium.

Appendix A. Optical properties of "astronomical" PAHs

The cross-section of PAHs in the visible and UV spectrum is written as a function of $x = 1 \, \mu m/\lambda$:

$$\sigma_C = 10^{-18} [p_1 f_v(x) + p_2 f_u(x)] C(x/x_c) \, cm^2/C. \qquad (A1.1)$$

The FUV component given by f_u has already been discussed in Section 3.2.1. A broad plateau starting at about $4 \, \mu m$ is used to represent the $\pi \to \pi^*$ transition that is observed in graphitic structures (Marchand 1987) as well as in mixtures of PAHs (Léger et al. 1989c):

$$f_v(x) = 1 \quad for \quad x \geq x_l = 4 \, \mu m^{-1}$$
$$= x^2(3x_l - 2x)/x_l^3 \quad for \quad x \leq x_l. \qquad (A1.2)$$

The polynomial in the last equality joins smoothly the plateau to a decrease in the emissivities proportional to λ^{-2} in the near IR like in graphite. A salient feature of the observed electronic absorption in PAHs is the cutoff, represented here by $C(x/x_c)$, that occurs at long wavelengths (Platt 1956, PLB). The cutoff wavenumber $x_c = 1.25(1 \, nm/a)$ is a function of the size of the molecule. Because a molecule may be elongated, it can have several cutoffs which we average by taking a cutoff $C(y) = \pi^{-1} \arctan(10^3(y - 1)^3)/y^3 + 0.5$ which is not as steep as a step function. The cutoff wavenumber is smaller for ionised PAHs (roughly by a factor of 3). PAHs have been assumed

ionised in reflection nebulae and HII regions (§ 4.3 and 4.4). The parameters p_1 and p_2 along with the abundances of PAHs Y_{PAH} have been matched with existing laboratory data and energy constraints as discussed in Section 3.3. In particular we have adopted $p_1 = 4.0$ and $p_2 = 1.1$.

The IR properties of PAHs are adapted from PLB and Léger and d'Hendecourt and Défourneau (1989b hereafter LHD). The cross-section of PAHs results from the contribution of three terms: 1) the electronic continuum (see formula (A1.1)) σ_{C1}; 2) the main features σ_{C2} at 3.3, 6.2, 7.7, 8.6, and 11.3 μm for which the integrated cross-sections are given by LHD (assuming a dehydrogenation of 40%) and the features width is based on observations of the reflection nebula NGC 2023 (Sellgren et al. 1985); 3) a pseudo-continuum below these features at wavelengths larger than about 10 μm that is due to numerous weaker features (LHD) that we approximate as the following cross-section per carbon atom:

$$\sigma_{C3} = \frac{A}{\lambda} e^{-(\lambda_m/\lambda)^2}, \qquad (A1.3)$$

where $A = 3.3 \times 10^{-20} \, cm^2 \, \mu m/C$, and $\lambda_m = 10 \, \mu m$, in order to explain qualitatively the near IR spectrum of the reflection nebula NGC 2023.

Appendix B Dust IR emission in various radiation fields

We present here the numerical tables (Table 6 to 9) of the IR emission computed for the modeled interstellar dust when it is embedded in various radiation fields. For each table, the first line is made of the center wavelength λ in μm of various IR filters: the first four filters have the IRAS response function (see *IRAS* Explanatory Supplement 1985); the next three filters are Dirac delta functions; the next two are near IR K and L' band filters (Glass 1973); the last column gives the parameter related to the intensity of the radiation field. Each group of four lines represents the IR emission (in MJy/sr/(10^{20} Hcm^{-2})) at one particular intensity of the radiation field, for respectively PAHs, VSGs, BGs, and total dust model for the abundances given in Table 2. Numbers in parenthesis are powers of ten. For example, the IR intensity emitted at 100 μm by BGs for $X = 0.5$ in Table 5 can be read as 2.85(-1) which is translated into 0.285 MJy/sr/(10^{20} Hcm^{-2}). Log-Log interpolation for intermediate values of the radiation field should give relatively accurate IR intensities. Detailed hypotheses concerning the radiation field follow.

References

Aitken, D. K.: 1981, in *IAU Symposium, Infrared Astronomy*, Ed. Wynn-Williams, C., and Cruikshank, D. P., p. 207

Allamandola, L. J., Tielens, A. G. G. M., and Barker, J. R.: 1985, *Astrophys. J. (Letters)*, **290**, L25

Allamandola, L. et al. : 1989, in *IAU Symp. 135 on Interstellar Dust*, ed. Allamandola, L. J., and Tielens, A. G. G. M., (Kluwer: Dordrecht), p. 129

Andriesse, C. D.: 1974, *Astron. Astrophys.*, **37**, 257

Andriesse, C. D.: 1978, *Astron. Astrophys.*, **66**, 169

Beichman, C. A.: 1987, *Ann. Rev. of Astron. Astrophys.*, **25**, 521

Bernard, J. P., Boulanger, F., Désert, and Puget, J. L.: 1990, in preparation

Bless, R. C., and Savage, B. D.: 1972, Astrophys. J., 10, 215

Bohlin, R. C., Savage, B. D., and Drake, J. F.: 1978, Astrophys. J., 224, 132

Boissé, P.: 1990, Astron. Astrophys., in press

Borghesi, A., Bussoletti, E., and Colangeli, L.: 1985, Astron. Astrophys., 142, 225

Boulanger, F. and Pérault, F.: 1988, Astrophys. J., 330, 964

Boulanger, F., Beichman, C., Désert, F. X., Helou, G., Pérault, M., and Ryter, C.: 1988, Astrophys. J., 332, 328

Boulanger, F.: 1989, in The Physics and Chemistry of Interstellar Molecular Clouds, Winnewisser G. and Armstrong J. T. (eds), Springer Verlag

Boulanger, F., Falgarone, E., Puget, J. L., and Helou, G.: 1990, Astrophys. J., submitted

Bussoletti, E., Colangeli, L., and Orofino, V.: 1987, Astrophys. J. (Letters), 321, L87

Butchart, I., Mc Fadzean, A. D., Whittet, D. C. B., Geballe, T. R., and Greenberg, J. M.: 1986, Astron. Astrophys., 154, L5

Cardelli, J. A., Clayton, G. C., and Mathis, J. S.: 1988, Astrophys. J. (Letters), 329, L33

Cardelli, J. A., Clayton, G. C., and Mathis, J. S.: 1989, Astrophys. J., 345, 245

Castelaz, H. W., Sellgren, K., and Werner, M. W.: 1987, Astrophys. J., 313, 853

Chini, R., Krügel, E., and Kreysa, E.: 1986, Astron. Astrophys., 167, 315

Chlewicki, G., and Laureijs, R. J.: 1988, Astron. Astrophys., 207, L11

Chlewicki, G., and Greenberg, M.: 1984, M.N.R.A.S., 210, 791

Chlewicki, G., and Greenberg, M.: 1989, Astrophys. J., submitted

Cohen, M. et al.: 1975, Astrophys. J., 196, 179

Cohen, M., Tielens, A. G. G. M., and Allamandola, L. J.: 1985, Astrophys. J. (Letters), 299, L93

Cox, P., and Leene, A.: 1986, in Space-Borne Sub-Millimetre Astronomy Mission, ed. ESA, p.177

Cox, P., and Leene, A.: 1987, Astron. Astrophys., 174, 203

Cox, P., Deharveng, L., and Leene, A.: 1990, Astron. Astrophys., 230, 181

De Groot, M. S., Van der Zwet, G. P., Jenniskens, P. M. M., Baas, R., and Greenberg, J. M.: 1988, in Dust in the Universe: Manchester Symp., ed. Bailey, M. E., and Williams, D. A., Cambridge Press, p. 265

de Muizon, M., Geballe, T. R., d'Hendecourt, L. B., and Baas, F.: 1986, Astrophys. J. (Letters), 306, L105

de Muizon, M., d'Hendecourt, L. B., and Geballe, T. R.: 1989, Astron. Astrophys., in press

Désert, F.X., Boulanger, F., Léger, A., Puget, J. L., and Sellgren, K.: 1986, Astron. Astrophys., 159, 328

Désert, F. X., Boulanger, F, and Shore, S. N.: 1986, Astron. Astrophys., 160, 295

de Vries, C. P.: 1985, Astron. Astrophys., 150, L15

d'Hendecourt, L. B., Léger, A., Olofsson, G., and Schmidt, W.: 1986, Astron. Astrophys., 170, 91

d'Hendecourt, L. B., and Léger, A.: 1987, Astron. Astrophys., 180, L9

Donn, B., and Khrishna Swamy: 1969, Physica, 41, 144

Draine, B. T., and Lee, H. M.: 1984, Astrophys. J., 285, 89

Draine, B. T., and Anderson, N.: 1985, Astrophys. J., 292, 494

Draine, B. T.: 1988, Astrophys. J., 333, 848

Draine, W. W., and Williams, D. A.: 1988, M.N.R.A.S, 231, 969

Duley, W. W., Jones, A. P., and Williams, D A.: 1989, M.N.R.A.S., 236, 709

Fabbri, R., Guidi, I., Natale, V., and Ventura, G.: 1986, in Proceed. of Marcel Grossman Meeting, Rome, June: 1985

Fitzpatrick, E. L., and Massa, D.: 1986, Astrophys. J., 307, 286

Fitzpatrick, E. L., and Massa, D.: 1988, Astrophys. J., 328, 734

Gatley, I., et al.: 1987, Astrophys. J. (Letters), 318, L73

Giard, M., Pajot, F., Lamarre, J. M., Serra, G., Caux, E., Gispert, R., Léger, A., and Rouan, D.: 1988, Astron. Astrophys., 201, L1

Giard, M., Pajot, F., Lamarre, J. M., Serra, G., Caux, E.: 1989, Astron. Astrophys., 215, 92

Gilra, D. P.: 1971, Nature, 229, 237

Glass, I. S.: 1973, M.N.R.A.S, 164, 155

Greenberg, J. M., and Hong, S. S.: 1974, in IAU Symp. 60: Galactic Radio Astronomy, ed. Kerr, F., and Simonson, S. C., p. 155

Greenberg, J. M.: 1982, in Submillimetre Wave Astronomy, ed. Beckman, J. E., and Phillips, J. P., Cambridge University Press

Greenberg, J. M., and Chlewicki, G.: 1983, Astrophys. J., 272, 563

Greenberg, J. M.: 1986, in Light on Dark Matter, ed. Israel, F. P., (Reidel: Dordrecht), p. 177

Guhathakurta, P., and Tyson, J. A.: 1989, in IAU Symp 139, Galactic and Extragalactic Background Radiation, ed. S. Bowyer, to appear

Hasegawa, H., and Koike, C.: 1984, in Laboratory and Observational Infrared Spectra of Interstellar Dust, ed. Wolstencroft, R. D., and Greenberg, J. M. (Royal Observatory: Edinburgh), p. 137

Hecht, J. H.: 1986, Astrophys. J., 305, 817

Hildebrand, R. H.: 1983, Quart. J. R. A. S., 24, 267

Hong, S. S., and Greenberg, J. M.: 1980, Astron. Astrophys., 88, 194

IRAS Explanatory Supplement: 1985, ed. Beichman, C. A., Neugebauer, H. J., Habing, H. J., Clegg, P. E., and Chester, T. J. (Washington, DC: US Government Printing Office)

Jenniskens, P. M. M., and Désert, F.-X.: 1990, in preparation

Lange, A. E., et al.: 1989, in IAU Symp. 135 on Interstellar Dust, ed. Allamandola, L., and Tielens, A. G. G. M. (Kluwer:Dordrecht) p. 499

Laureijs, R. J., Mattila, K., and Schnur, G.: 1987, Astron. Astrophys., 184, 269

Laureijs, R. J.: 1989, Thesis, Groningen

Leene, A., and Cox, P.: 1987, Astron. Astrophys., 174, L1

Léger, A., and Puget, J. L.: 1984, Astron. Astrophys., 137, L5

Léger, A., Jura, M., and Omont, A.: 1985, Astron. Astrophys., 144, 147

Léger, A., and d'Hendecourt, L.: 1987, in PAHs and Astrophysics, ed. Léger, A., d'Hendecourt, L., and Boccara, N., (Kluwer Acad. Publ. Group: Dordrecht), p. 223

Léger, A., Boissel, P., Désert, F. X., and d'Hendecourt, L.: 1989a, Astron. Astrophys., 213, 351

Léger, A., d'Hendecourt, L. and Defourneau, D.: 1989b, Astron. Astrophys., 216, 148 (LHD)

Léger, A., et al.: 1989c, in IAU Symp. 135 on Interstellar Dust, ed. Allamandola, L., and Tielens, A. G. G. M., p. 173

Lequeux, J.: 1989, in Recent developments of Magellanic Cloud

research, de Boer, K. S., Spite, F., and Stasinska, G. (eds), p. 119

Lillie, C. F., and Witt, A. N.: 1976, *Astrophys. J.*, **208**, 64

Marchand, A.: 1987, in *PAHs and Astrophysics*, ed. Léger, A., d'Hendecourt, L., and Boccara, N., (Kluwer Acad. Publ. Group: Dordrecht), p. 31

Massa, D., and Savage, B. D.: 1989, in *Interstellar Dust, Allamandola L. J., and Tielens, A. G. G. M. (eds) (Kluwer:Dordrecht)

Mathis, J. S., Rumpl, W., and Nordsieck, K. H.: 1977, *Astrophys. J.*, **217**, 425 (MRN)

Mathis, J. S., Merger, P. G., and Panagia, N.: 1983, *Astron. Astrophys.*, **128**, 212

Mathis, J. S., and Whiffen, G.: 1989, *Astrophys. J.*, **341**, 808

Matsumoto, T., et al.:1988, *Astrophys. J.*, **329**, 567

Merger, P., Chini, R., Kreysa, E., and Wink, J.: 1987, *Astron. Astrophys.*, **182**, 127

Meyer, J.-P.:1979, in *Les éléments et leurs isotopes dans l'Univers, 22nd Liège International Astrophysical Symposium*, (Liège: University of Liège Press), p. 153

Morgan, D. H.: 1980, *M.N.R.A.S.*, **190**, 825

Omont, A.: 1986, *Astron. Astrophys.*, **164**, 159

Pajot, F., Gispert, R., Lamarre, J. M., Peytureaux, R., Puget, J. L., Serra, G., Coron, N., Dambier, G., Leblanc, J., Moalic, J. P., Renaud, J. C., and Vitry, R.: 1986, *Astron. Astrophys.*, **154**, 55

Pajot, F., Boissé, P., Gispert, R., Lamarre, J. M., and Puget, J. L.: 1986, *Astron. Astrophys.*, **157**, 393

Pérault, M., Boulanger, F., Falgarone, E., and Puget, J. L.: 1989, *Astrophys. J.*, submitted

Platt, J. R.: 1956, *Astrophys. J.*, **123**, 486

Price, J.: 1981, *Astron. J.*, **86**, 193

Puget, J. L., Léger, A., and Boulanger, F.: 1985, *Astron. Astrophys.*, **142**, L19 (PLB)

Puget, J. L., and Léger, A.: 1989, *Ann. Rev. Astron. Astrophys.*, **27**, 161

Rice, W., Boulanger, F., Viallefond, F., Freedman, W., and Soifer, B. T. 1989, *Astrophys. J.*, in press

Rieke, G. H., and Lebofsky, M. J.: 1985, *Astrophys. J.*, **288**, 618

Rowan-Robinson, M.: 1986, *M.N.R.A.S.*, **219**, 737

Ryter, C., Puget, J. L., and Pérault, M.: 1987, *Astron. Astrophys.*, **186**, 312 (RPP)

Ryter, C., and d'Hendecourt, L. B.: 1989, preprint

Sakata, A., Wada, S., Okutsu, Y., Shintani, H., and Nakoda, Y.: 1983, *Nature*, **301**, 493

Sakata, A., Wada, S., Tanabé, T, and Onaka, T.: 1984, *Astrophys. J. (Letters)*, **287**, L51

Salisbury, D. W., Allen, J. E., Donn, B., Moore, W. J., and Khanna, R. K.: 1987 in *Carbon in the Galaxy*, (NASA Ames conf. proc.)

Savage, B. D., and Mathis, J. S.: 1979, *Ann. Rev. Astron. Astrophys.*, **17**, 73

Seab, C. G., Snow, T. P., and Joseph, C., L.: 1981, *Astrophys. J.*, **246**, 788

Seab, C. G.: 1987, in *Interstellar Processes*, ed. Hollenbach, D. J., and Thronson, H. A. (Reidel: Dordrecht), p. 491

Sellgren, K.: 1981, *Astrophys. J.*, **245**, 138

Sellgren, K., Werner, M. W., and Dinerstein, H. L.: 1983, *Astrophys. J. (Letters)*, **271**, L13

Sellgren, K.: 1984, *Astrophys. J.*, **277**, 623

Sellgren, K., Allamandola, L. J., Bregman, J. D., and Wooden, D. H. 1985, *Astrophys. J.*, **299**, 416

Sellgren, K.: 1989, in *IAU Symp. 135: Interstellar Dust, Allamandola, L. J., and Tielens, A. G. G. M. (eds), (Kluwer: Dordrecht) p.103

Seki, J., and Yamamoto, T.: 1980, *Astrophys. Sp. Scie.*, **72**, 79

Sitko, M. K., Savage, B. D., and Meade, M. R.: 1981, *Astrophys. J.*, **246**, 161

Soifer, B T., Russell, R. W., and Merrill, K. M.: 1976, *Astrophys. J. (Letters)*, **207**, L83

Stecher, T. P.: 1969, *Astrophys. J. (Letters)*, **157**, L125

Tielens, A. G. G. M., and Allamandola, L. J.: 1987, in *Interstellar Processes*, ed. Hollenbach, D. J., and Thronson, H. A. (Reidel: Dordrecht) p. 397

Ungerechts, H., and Thaddeus, P.: 1987, *Astrophys. J. Suppl.*, **63**, 645

Van de Hulst, H. C.: 1957, *Light scattering by small particles*, (Wiley:New York)

Walterbos, R. A. M., and Schwering, P. B. W.: 1987, *Astron. Astrophys.*, **180**, 27

Waters, L. B. F. M., et al.: 1989, *Astron. Astrophys.*, **211**, 208

Weiland, J. L., Blitz, L., Dwek, E., Hauser, M. G., Magnani, L., and Rickard, L. J: 1986, *Astrophys. J. (Letters)*, **306**, L101

This article was processed by the author using Springer-Verlag TEX AA macro package 1989.